University of Stavanger

Faculty of Science and Technology

MASTER'S THESIS

Study program/ Specialization: M.Sc. in Offshore Technology, Marine and Subsea Technology	Spring semester, 2015 Restricted access
Writer: Marianne Klepp Andersen	…… (Writer's signature)

Faculty supervisor: Arnfinn Nergaard

External supervisor(s): Wolfgang Mathis (NeoDrill)

Thesis title:

Analysis of Forces in a Subsea Wellhead System Supported by NeoDrill Conductor Anchor Node

Credits (ECTS): 30

Key words: Wellhead and conductor system Conductor Anchor Node (CAN) Wellhead Support Frame (WSF) Bending Moment Fatigue	Pages: 90 + Enclosure: 1 Stavanger, 15/06-2015 Date/year

PREFACE

The work presented in this Master's thesis has been carried out at the Department of Mechanical and Structural Engineering and Materials Science, University of Stavanger (UiS), as a part of the two-year master's degree program Offshore Technology. The report has been written during the last semester and is weighted with 30 units.

The thesis consists of two parts. Part I is a literature study of various topics that are of relevance for the report. Part II consists of analysis, results, discussion, and conclusion. The analysis in this thesis is performed in the computer software OrcaFlex. During the work of this thesis, I have failed and learned several times. It has been an educational process, which has taught me work methods, independent work and time prioritizing.

It is assumed that the reader of this report has a certain understanding of terminologies used in the thesis.

I want to give a special thanks to my supervisor, Professor Arnfinn Nergaard, for guidance with the thesis. Arnfinn has taken the time to help and guide me when it has been necessary. I would also like to thank my external supervisor at NeoDrill, Wolfgang Mathis, for the support and guidance during the work. PhD student Adekunle Orimolade also deserves big thanks for giving me good advices on how to build my model in OrcaFlex. Last but not least, I want to thank my fellow students in room D-258. They have contributed to good spirits throughout the process.

Stavanger, June 15th, 2015

Marianne Klepp Andersen

ABSTRACT

During drilling operations the marine drilling riser is exposed to environmental loads like waves and currents, as well as loads from the rig. These environmental loads are transferred from the riser to the wellhead system. Large bending loads will occur along the wellhead and conductor system. The loads will fluctuate in time and can cause fatigue damage accumulation at connectors and welds present in the system. At present, the fatigue performance is believed to be a concern for a growing number of operations. This report investigates how the distribution and magnitude of the bending loads will change in different conditions. This is done to identify a method to achieve an optimum distribution and position of critical bending moments. Additionally, a discussion on whether a change in distribution and magnitude of the bending moments will reduce fatigue accumulation in critical points is given.

A global riser analysis is conducted using the computer software OrcaFlex to study how the bending moments behave under different conditions. The analysis is run for three different scenarios with the intention of comparing results.

The results show that the bending moments will behave differently under various conditions. In soft soils, the largest bending moments will occur at a depth of 5 to 10 meters below the seabed surface. Furthermore, it is shown that the magnitude of the bending moments will increase in soft soils. The weight of the blow out preventer will also affect the bending moments. In soft soils, the lateral resistance is reduced, thus a lager lateral displacement of the blow out preventer can occur. The aforementioned can cause fatigue accumulation along critical hotspots within the wellhead and conductor system. The conductor anchor node is designed to carry heavy blow out preventers and gives the system a high lateral stiffness. The large bending moments occurring below the seabed surface will be reduced when the conductor anchor node is applied. The conductor anchor node will most likely reduce the fatigue accumulation at critical points below the seabed. Larger bending moments will occur on top of the conductor anchor node and will most likely expose connectors and welds above the seabed for somewhat increased fatigue damage.

A wellhead support frame can be installed on top of the conductor anchor node to support the high-pressure wellhead. The wellhead support frame will increase the systems stiffness, thus larger bending moments will occur on top of the wellhead support frame. The results give a clear indication that a redistribution and change in magnitude of the bending moments are achievable. The conductor anchor node gives the engineers a tool enabling an optimized system for maximum fatigue life below seabed surface. Without the conductor anchor node there is no possibility to change the characteristics of the seabed. However, it is difficult to identify one method to achieve an optimal distribution and position of bending moments, but it is possible to redistribute the bending moments and shift the problem to less critical locations in the system.

CONTENTS

LIST OF FIGURES

LIST OF TABLES

ABBREVIATIONS

BOP	Blow Out Preventer
CAN™®	Conductor Anchor Node
LMRP	Lower Riser Marine Package
LPWHH	Low Pressure Wellhead Housing
MODU	Mobile Offshore Drilling Unit
MSL	Mean Sea Level
VIV	Vortex Induced Vibration
WH	Wellhead
WHH	Wellhead Housing
WSF	Wellhead Support Frame

CHAPTER 1

1 INTRODUCTION

Wellhead (WH) and conductor fatigue is an increasing issue regarding offshore drilling operations. According to DNV (2011) there are no international codes or standards that provide guidance on how subsea WH fatigue assessments shall be carried out. Several papers are written about the large bending loads and the fatigue issues arising in the WH and conductor system. Some of these papers also suggests how to mitigate the problems. Nevertheless, few publications can be found about the Conductor Anchor Node (CAN) and the Wellhead Support Frame (WSF) concept. This study therefore aims to highlight how the CAN and the WSF can change the distribution and maximum values of the bending moments, thus improving the fatigue accumulation in the WH and conductor system.

A subsea WH acts as the interface between the marine drilling riser, the conductor and its internal casings. The marine drilling riser is subjected to environmental loads like waves and currents as well as loads from the rig. These loads are transferred down the riser to the WH and conductor system and can cause fatigue issues at critical welds and connectors. Over the last few years, the potential for severe fatigue loading of the WH and conductor system has increased due to the use of heavier Blow Out Preventers (BOP) and longer well operations. Because of this, there is a growing need to improve the fatigue life of the critical welds and connectors in the system.

Previous work has shown that heavier BOPs and soft soils will increase the bending moments along the WH and conductor system, thus increasing the fatigue accumulation in critical

hotspots along the system. In a paper written by Lim et al. (2012) the authors suggest measures to mitigate these large bending moments in critical areas, hence improving the fatigue accumulation in critical hotspots. These mitigating measures include relocation of the conductor and casing connector, increase conductor wall thickness or diameter, increase casing wall thickness, utilize a rigid lockdown WH, improve the weld quality, avoid additional welds and improve the connector fatigue details.

In this thesis, a new way of reducing and redistribute the large bending moments below seabed surface is studied. The CAN and WSF will reduce and redistribute the large bending moments occurring below the seabed surface. This will most likely improve the fatigue performance of critical components located in this area.

A global riser analysis is performed using the computer software OrcaFlex. The analysis is run for three different models: i) conventional installed conductor, ii) conductor installed inside the CAN and iii) conductor installed inside the CAN with the WSF supporting the high-pressure wellhead.

1.1 BACKGROUND

Offshore drilling activities are usually carried out using drilling risers with subsea BOP stacks deployed from mobile drilling units. The risers are exposed to wave-induced motions both from direct wave loading and vessel motions, as well as vortex-induced vibrations due to current flow past the risers. These motions are transferred from the riser to the WH, conductor and casing system and can cause fatigue issues at critical connectors and welds. Over the last few years, the potential for severe fatigue loading of the WH system has increased. Analytical predictions of fatigue in subsea WHs is such that fatigue performance is believed to be a concern for a growing number of operations. The various factors contributing to this includes: i) use of modern drilling rigs with larger BOP stacks, ii) operations in new and harsher environments where the drilling riser system must withstand greater environmental loads, and iii) more complex well operations which results in longer periods where the drilling riser is connected to the WH (Lim et al., 2012).

A new suction anchor type well foundation concept has been developed to diminish these negative impacts. The CAN unit provides adequate load capacity for carrying heavy BOPs safely. In this manner, the CAN protects the well from fatigue capacity consumption during drilling. The concept also allows pre-rig conductor installation, which is a major advantage in reducing rig time; additionally, it reduces cost for top-hole construction and rig failure risk exposure. By mobilizing substantial carrying capacity from the soil through the CAN's large cross sectional area and captured soil mass, it will reduce the risk of the well becoming over-loaded by undesired, accidental loads. This is an important aspect in view of risk mitigation and improving possibilities of applying contingency means in case of undesired events or disasters (Sivertsen & Strand, 2011).

1.2 OBJECTIVES

A marine drilling riser is exposed to environmental loads, as well as loads from the drilling rig. These loads are transferred from the drilling riser to the BOP stack and further down to the WH and conductor system. This will cause large bending moments from the base of the wellhead housing (WHH) to a depth of 10 to 15 meters below seabed surface. These bending moments shall be distributed over a system with variable geometry, thus the localization of the bending loads is important for the integrity.

NeoDrill designs and provides a subsea well foundation called CAN. The CAN gives lateral support to the system leading to a new distribution of the bending moments. NeoDrill has also developed a WSF that can be installed on top of the CAN to support the high-pressure WH. This configuration will redistribute the bending moments further.

One objective of this thesis is to investigate how the distribution and maximum value of the bending moments will change due to the CAN and the WSF. This is done to identify a method to achieve an optimum distribution and position of critical bending moments. Another objective is to study how the bending moments change due to different soil stiffness and BOP weights. The last objective in this thesis is to perform a qualitative assessment of how fatigue performance is affected due to the change in bending moments.

1.3 STRUCTURE OF THESIS

This subchapter will give a short explanation of the 11 chapters included in this thesis. The report starts with a literature study of various topics that are of relevance to the thesis. This is done to provide an insight and an overall understanding of the relevant theory. Further, a global riser analysis is performed using the software OrcaFlex. The four last chapters in this report contains results, discussion, conclusion and suggestions for further work.

Chapter 1: Introduction

This is an introduction to the topic. Explanation of the objectives of the thesis and its structure is given in this chapter.

Chapter 2: Present Practice

In this chapter an overview of the drilling process is given. The different components of a typical drilling system are briefly explained.

Chapter 3: Description of NeoDrill Technology

A short description of the NeoDrill technology and how the CAN works.

Chapter 4: Environmental Loads

Chapter 4 gives a short overview of different environmental loads that will affect the drilling system.

Chapter 5: Fatigue

In this chapter an introduction to fatigue is given, with emphasize on fatigue accumulation in the WH and conductor system.

Chapter 6: OrcaFlex Theory

The theory behind OrcaFlex is explained in this chapter.

Chapter 7: Methodology and Modeling

This chapter contains a short section of methodology used in ISO 13624-2 on how riser analysis should be performed. A description of the different mechanical models is given. It also contains a description of how the model is built in OrcaFlex and a verification of the model is given.

Chapter 8: Results

Presentation of the results obtained from the analysis.

Chapter 9: Discussion

A discussion of the results presented is given in this chapter.

Chapter 10: Conclusion

Chapter 10 gives a short summary of the results and presentation of the conclusion drawn from them.

Chapter 11: Suggestions for further work

Suggestions for objectives that could be investigated in future studies.

1.4 LIMITATIONS

To be able to perform calculations in a computer program simplifications are needed, which in turn will cause limitations. This will make the model deviate from the reality. It is important to keep the physical properties correct in the transition from reality to model. One challenge when creating a model is to reproduce the reality as accurate as possible, which can be difficult to do without all data available. In this thesis a model is built in OrcaFlex with the aim to do a dynamic analysis of the drilling system. The model is created with the intention of reproducing the physical properties of a real-life system.

With the above-mentioned in mind, it is important to point out that the results obtained in OrcaFlex may differ from reality. The environmental conditions implemented in the analysis are not real values obtained from a specific field. Waves and current will vary with time, thus affecting the system in different ways. If measured values for waves and currents were implemented in the model the results would most likely be different. In this report, P-Y curves are not available and a soil investigation to obtain values for different soil types is an extensive topic, thus not manageable in the time perspective of this thesis. As this is not included in the model, results may differ from a real-life system.

CHAPTER 2

2 PRESENT PRACTICE

Offshore drilling activities began early in the 20th century when shallow water fixed platforms were used to access offshore reservoirs. However, it was not until after 1947, when the first offshore well was drilled at a location far away from land, that the offshore drilling and production became widely viable. The following chapter provides a brief description of the drilling process. The drilling process will vary from operation to operation, but in the first section of this chapter a general description is given. A description of different components in a drilling system is provided in the next sections.

2.1 THE DRILLING PROCESS

The drilling process is done in stages. Casings with decreasing diameter sizes are lowered into the drilled hole and cemented in place, see figure 2-1.

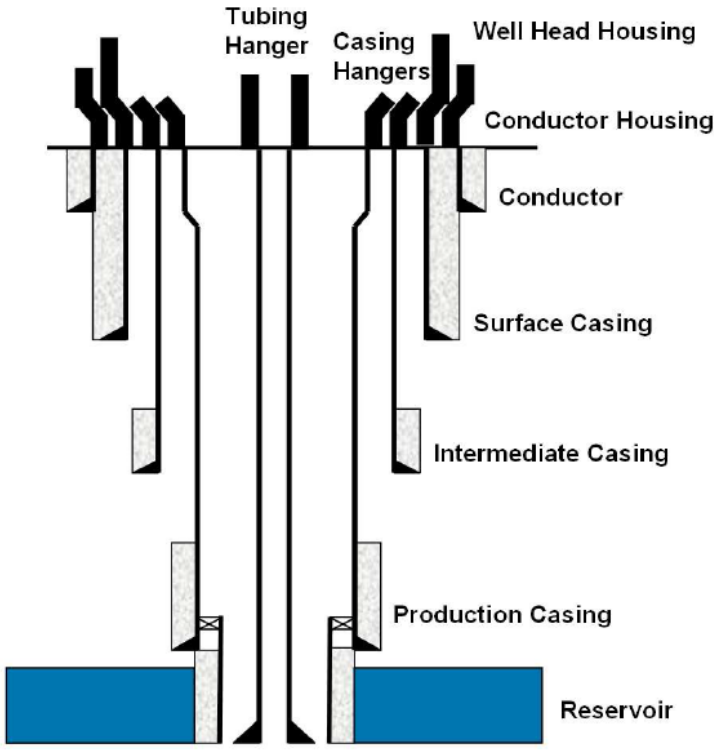

Figure 2-1 Typical well construction in the North Sea (DNV, 2011)

The first step of the drilling process is to lower the guide base. The guide base is connected to four guidelines, which will be used for lowering the components in the next steps. This will ease the operation and the position of the next components will be more precise.

The next step is to start the drilling; a 36" hole is drilled and fitted with a 30" conductor casing. The 30" conductor casing is cemented in place and a permanent guide base is installed. The upper part of the conductor is the low-pressure housing. For wells with high loads a 42" hole is drilled and fitted with a 36" conductor.

A 26" hole is drilled for the 20" casing. The 20" casing is commonly equipped with a 18 3/4" WH. Drilling of the 36" hole and the 26" hole does not require complete circulation of the drill mud, thus a drilling riser is not needed. In this phase, drill cuttings from the borehole are typically circulated and disposed at the seabed. The marine drilling riser and the BOP are

connected to the WH after the 20" casing has been cemented in the hole. The marine drilling riser and the BOP will stay in place for the rest of the drilling operation.

The next casings will decrease in size until the anticipated depth has been reached, e.g. the 20" casing is followed by a 13 3/8", then a 9 5/8" and a 7" casing. For all these last casings the drilling riser will be used to divert the drilling fluid back to the rig where cuttings are removed and a clean drilling fluid will be circulated back to the borehole (Torbergsen et al., 2012).

2.2 SYSTEM COMPONENTS

The drilling process involves a drilling system and several components are necessary for drilling a well. Some of these components are located on the rig and others are situated beneath the water surface. Figure 2-2 shows the general components of a drilling system. Each of these components will be presented in the following sub-sections.

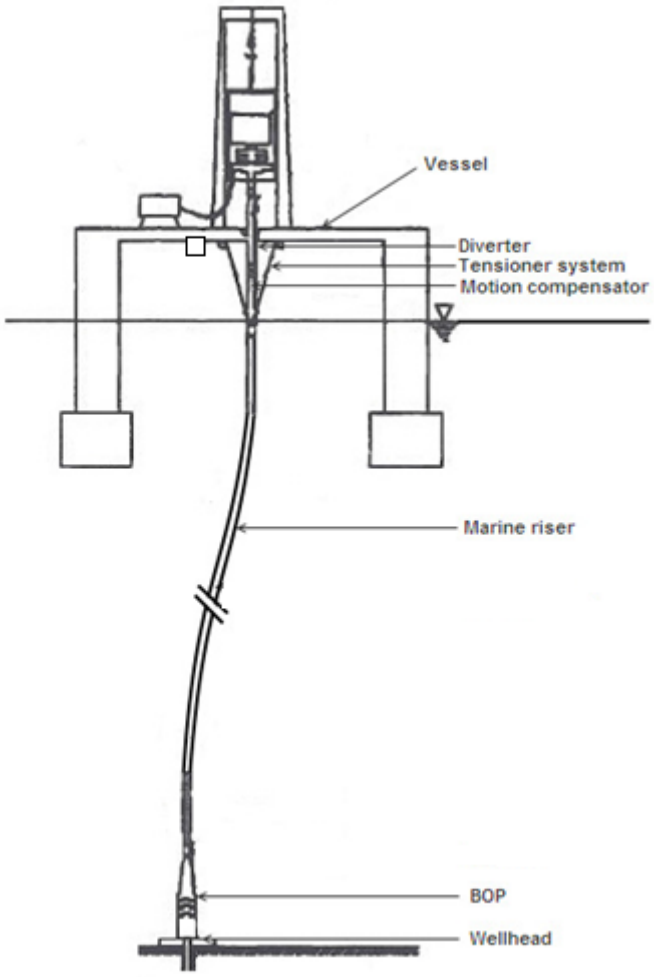

Figure 2-2 Components of a drilling system (Stokvik, 2010)

2.2.1 Motion compensation system

A vessel has six motions that are typically referred to as degrees of freedom. These motions are heave, sway, surge, pitch, roll and yaw. All these motions will affect the drilling operation. Heave is usually the most critical. To compensate for the vertical movement of a drilling rig due to heave a floating drilling rig has motion-compensating equipment. This equipment consists of guide line and pod line tensioners, drill string compensator and riser tensioners (Bai et al., 2005).

2.2.2 Riser tensioner

The riser tensioner system prevents the riser from buckling. Riser tensioners are attached to the outer barrel of the slip joint with wire ropes. Tensioners support the riser, and the mud within it, with a persistent tension as the rig heaves. Since the riser is connected to the WH, it is important that the tensioners can manage differential movement between the riser and the rig. When the rig rises the riser will stretch and when the rig moves downward the riser will buckle if a tensioner is not installed (Malm Orstad AS, 2015).

2.2.3 Diverter

According to API (1991) the diverter is:

"A device attached to the wellhead or marine riser to close the vertical access and direct any flow into a line and away from the rig"

The diverter is similar to a low-pressure BOP and is used to protect against shallow gas kicks during drilling operations. The system function is to direct fluids flowing from the well away from the rig. If gas or other fluid from shallow gas zones enter the hole under pressure, the diverter will close around the drill pipe and the flow is diverted away from the rig (Bai & Bai, 2005).

2.2.4 Marine riser

The riser is a conductor pipe that connects the vessel on the surface to the well at the seabed. Risers are mainly used for four purposes: drilling, completion/workover, production/injection and export (Sparks, 2007). In this thesis a tensioned drilling riser is selected for the analysis. A more detailed description of the marine drilling riser will be given in section 2.3.

2.2.5 Choke and kill lines

Choke and kill lines are attached to the outside of the main riser pipe. By pumping heavier mud into the hole, high pressure is circulated out of the wellbore through the choke and kill lines. If it is not possible to get the pressure under control with heavy mud, the well is killed by pumping cement down the kill line. The drill string enables circulation of liquid mud. The central functions of the mud are to cool the bit, lubricate the drill string, prevent wall cave-ins, provide hydrostatic pressure and keep the hole free of cuttings by forced circulation (Bai et al., 2012).

2.2.6 Lower marine riser package

The Lower Marine Riser Package (LMRP) is the interface between the BOP stack and the riser system. The main function of the LMRP is to provide disconnect of the riser from the BOP in an emergency situation (McCrae, 2003).

2.2.7 Blow out preventer

A BOP is a large specialized valve used to control and seal an oil or gas well. During drilling operations, a BOP is installed just above the seabed. It is the connection between the riser and the WH. The BOP may be closed if the drilling crew loses control of formation fluids. By closing the valves, the drilling crew normally regains control of the reservoir. After regaining control of the reservoir procedures can be initiated to increase the mud density until it is possible to open the BOP and retain pressure control of the formation (Subsea 1, 2010). The BOP will shut in the well under pressure so that formation fluids that have moved into the wellbore can be circulated out of the well while continuous control is maintained (Sheffield, 1982).

2.3 THE MARINE DRILLING RISER

The marine drilling riser system is the communication link between the rig and the BOP. The primary functions of the system are to guide tools into the well, support choke, kill, and auxiliary lines and provide fluid communication between the well and the drilling rig (API 16F). This section will give a general description of the components of a marine drilling riser. All components are shown in figure 2-3.

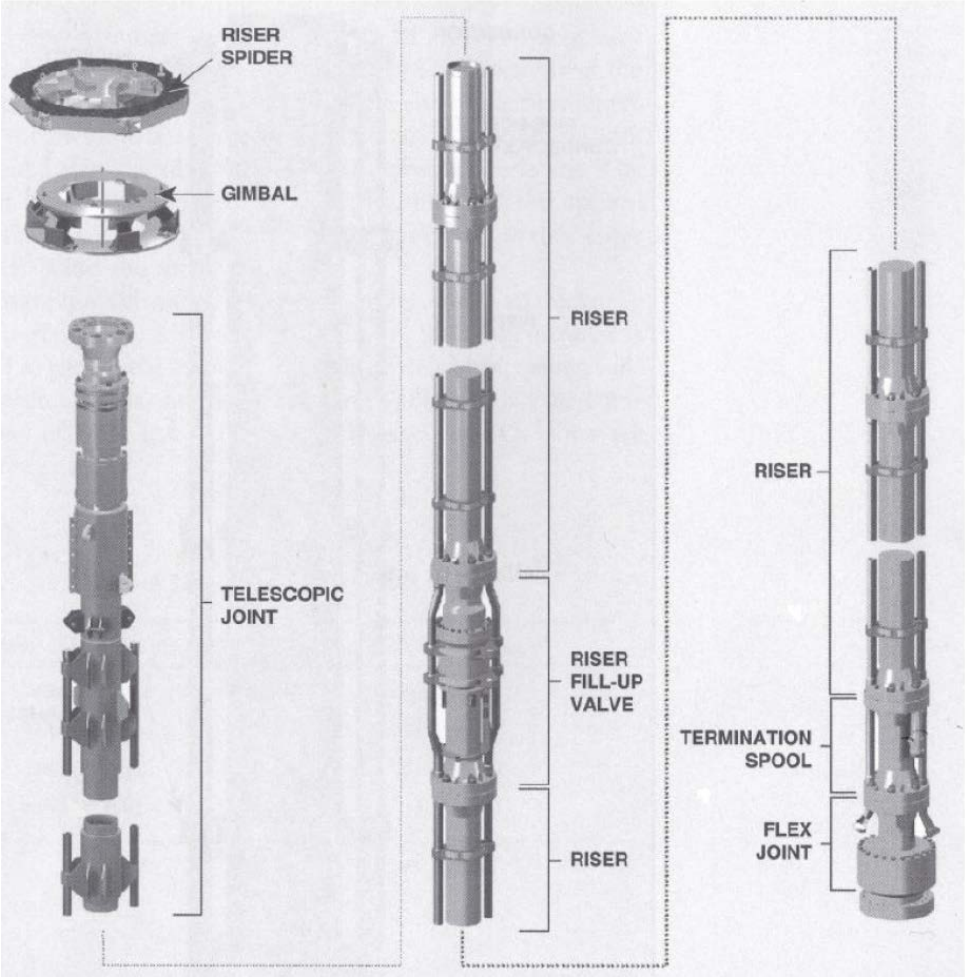

Figure 2-3 Components of Marine Drilling Riser (Bai & Bai, 2005)

The spider is normally located in the rotary table on the drill floor. Its function is to support the riser as the pipe is being lowered into or pulled out of the water.

A gimbal is installed between the spider and the rotary table. This device will allow the vessel to pitch and roll without distorting the riser.

The diverter, described in section 2.2.3, is located between the slip joint and the drill floor. The slip joint, or telescopic joint, compensates for the heave of the rig. A slip joint consists of an inner barrel that slides into an outer barrel. The inner barrel is connected to the rig and the outer barrel is connected to the riser joints. The slip joint is designed to prevent damage to the riser and control umbilical where they pass through the rotary table. It also protects the riser from damage due to rig heave (Bai & Bai, 2005; Sheffield, 1982).

A riser joint is a large diameter, high strength pipe with mechanical connectors welded to each end. Riser joints are the main components that make up the riser. When the riser system is being deployed, the riser joints are coupled on the drill floor and lowered into the sea. Their function is to extend the riser system to the sea floor. The length of each joint can vary from 30 ft. to 75 ft. Length, wall thickness and weight of these pipes depends on the water depth of the operation. Kill and choke lines are attached to the outside of the joints (Bai & Bai, 2005).

Kill and choke lines are attached to the outside of the main riser pipe and are used to control high-pressure situations. Kill and choke lines are described in section 2.2.5.

Flex joints are reducing the bending moment on the riser by allowing angular displacement between the riser and the BOP stack. Flex joints can also be used at the top of the riser to allow motions of the rig, or at some intermediate level below the slip joint to reduce stresses in the riser (API, 2010).

Buoyancy or floating modules can be connected to the riser to decrease the tension required at the surface. The two common types of modules are thin-walled air cans and fabricated syntactic foam (Bai & Bai, 2005).

2.4 SUBSEA BOP SYSTEM

The subsea BOP system is located between the drilling riser and the WH. It is designed to assist in well control and to shut in the well if the well starts to flow due to influx of formation fluids. Subsea BOP stacks are made up of several components. Such stacks allows the personnel to have control of a well under virtually every condition that is likely to occur. The BOP stack is run from surface on the marine drilling riser and attached to the WH on the ocean floor (McCrae, 2003).

BOPs come in a variety of sizes, styles and pressure ratings. Some are designed to seal around tubular components, some can close over an open wellbore and others can cut through the drillpipe. BOPs are divided into two main categories (Subsea 1, 2010):

- Annular blow out preventer
- Ram blow out preventer

The majority of BOP stacks have at least one annular BOP at the top and two or more ram-type preventers below (Subsea 1, 2010). There are four types of ram preventers: pipe rams, blind rams, shear rams and blind shear rams. Usually at least two ram preventers are mounted in the BOP stack (Hossain, 2011).

The BOP is an important component in the drilling system, but it exposes the WH system to major loads. According to Lim et al. (2012), the BOP stacks of the new 5th and 6th generation drilling vessels are up to 1.6 times longer and 2 times heavier than the BOP stacks on older 3rd or 4th generation vessels.

2.5 SUBSEA WELLHEAD AND CONDUCTOR SYSTEM

The subsea WH is located at the seabed and is the connection between the BOP and the well. The WH and conductor system is a key load bearing structure that supports the BOP stack and the various casings. The exact architecture of the system will vary, though there are some components that are common for all systems. Figure 2-4 illustrates a general arrangement of a WH and conductor system which consists of the following components (Greene & Williams, 2012):

- 30" or 36" conductor which is the outermost tubular
- Low pressure wellhead housing (LPWHH)
- 18 5/8" or 20" high pressure casing
- High pressure WH
- Tubing hanger
- Various casing and completion strings
- Conductor and casing connectors

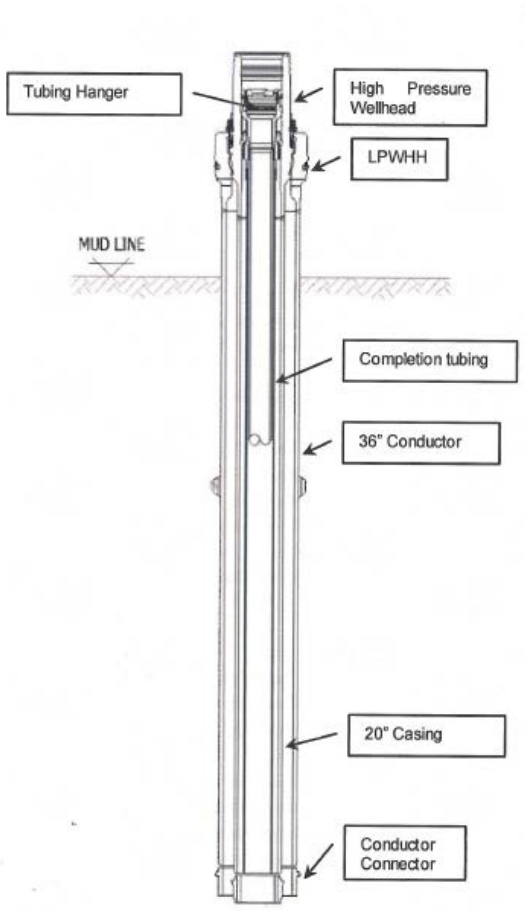

Figure 2-4 Illustration of a typical WH and conductor system (Greene & Williams, 2012)

The subsea WH, together with the BOP, provides the means to safely contain reservoir pressure during drilling and production. The WH must be designed for high structural loads imposed during drilling, well completion or workover operations. In addition, it must support the weight of the BOP and casing, drilling riser loads and forces imposed by internal pressure (Richbourg et al., 1998).

CHAPTER 3

3 DESCRIPTION OF NEODRILL TECHNOLOGY

NeoDrill is a Norwegian offshore service company located at Ålgård. The company was founded in 2000 and has currently four employees. In 2000, the company's general manager, Harald Strand, developed an innovative suction anchor called CAN. This chapter gives a description of the CAN, how it is installed and what benefits the technology provides. The concept is designed for exploration and production well requirements. NeoDrill's technology has been applied for conventional as well as more technical challenging wells in various fields on the Norwegian Continent Shelf (NeoDrill, 2015).

3.1 INTRODUCTION

Suction anchors have been in use in the oil and gas industry for several years, and over the last decade NeoDrill has developed an innovative approach to top-hole well construction. The company has developed a new well foundation named CAN. Figure 3-1 shows the CAN, which is a large cylinder with an open end and a concentric center pipe/conductor guide, which extends as deep as the CAN's skirt. The CAN eliminates the weak link in current well design by guiding the conductor during installation and giving it mechanical support after installation. In this way the conductor is turned into a very high lateral load capacity and bending stiff construction. In addition, the CAN will reduce the risk of the well becoming over-loaded by unwanted accidental loads, e.g.: because of a rig drift off/drive off situation. This is made possible by mobilizing considerable carrying capacity from the soil through the CAN's large cross sectional area and captured soil mass (Sivertsen & Strand, 2011).

According to Sivertsen & Strand (2011) the concept will reduce rig time as it enables pre-rig installation of the conductor, thus reducing top-hole construction costs and rig failure risk exposure. A number of full-scale applications on the Norwegian Continental Shelf has validated the advantages and viability.

Figure 3-1 NeoDrill CAN development (NeoDrill, 2012)

3.2 NEODRILL TECHNOLOGY

As mentioned earlier the CAN is a specially designed suction anchor type of structure that consists of an open-ended cylindrical outer shell and a conductor guide. According to Sivertsen & Strand (2011) a typical CAN weight will be in the range of 60 to 80 tons, with a diameter varying from 5 to 6 meters and the height ranging from 8 to 12 meter. Figure 3-2 shows a typical stack-up of a CAN/conductor system.

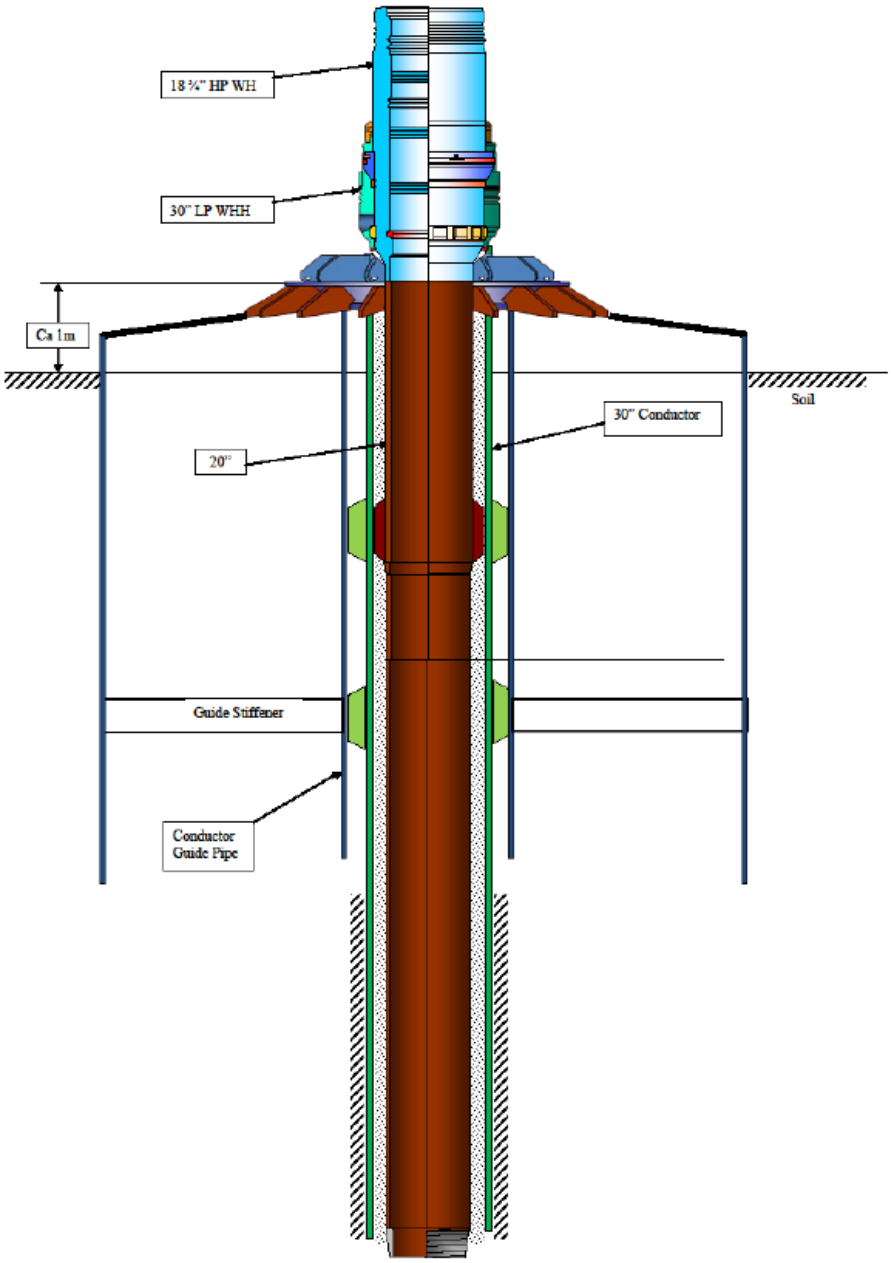

Figure 3-2 Typical stack-up of CAN/conductor (Sivertsen & Strand, 2011)

The CAN is pre-installed by a vessel fitted for the operation. A dynamic positioning system and a crane with a heave compensator are required to install the CAN. At location, the CAN is

picked up by the crane and lowered to a location near the seabed. The CAN is placed on the seabed where it self-penetrates into the soil. A ROV (Remotely Operated Vehicle) equipped with a suitable pump is docked to the CAN to pump out captured water to reduce the CANs internal pressure. In this way, the achieved pressure differential will generate a net downward directed force, which will push the CAN further into the sediments. Because of the CAN's large contact area to the soil, it is capable of carrying the entire BOP stack and casing loads (Sivertsen & Strand, 2011).

The same vessel that is used to install the CAN, can also be utilized to undertake the conductor installation. The conductor is preassembled onshore, and in one simple crane operation the conductor is lifted horizontally off the deck and lowered into the water. Thereafter, it is rotated to a vertical position before it is run and stabbed into the CAN conductor guide to self-penetrate. A hydraulic hammer is used to drive the conductor into the soil until landing its WHH in the CAN (Sivertsen & Strand, 2011).

NeoDrill claims that the CAN technology provides (NeoDrill, 2015):

- Less rig time – cost efficient solutions
- Extended well fatigue life
- Proven technology
- Increased axial and lateral load capacity
- Increased bending, fatigue and accidental load capacity
- "Fast track" field development – accelerated production enabled
- Reduced environmental footprint
- HMS-improvement – less manual handling of heavy equipment
- Risk mitigation – according to ALARP

CHAPTER 4

4 ENVIRONMENTAL LOADS

It is important to understand the loads acting on the drilling system in order to understand the damage that may occur in the system. In this chapter a short description of the environmental loads acting on the drilling system is given. Wind, waves and current acts on the rig during drilling operations and these environmental loads induce on the riser and on the connection to the bottom a combination of axial and lateral forces and bending moments. The load history of a system is affected by the environmental conditions during drilling operations. The environmental loads fluctuates in time and generates a dynamic loading regime, thus causing fatigue damage accumulation in the weaker points in the top part of the WH and conductor system (Schaer & Gaschen, 2013). Wind loads will not be discussed in this chapter, as it will not affect the drilling riser to the same extent as waves and current.

4.1 LOADS ON THE DRILLING SYSTEM

The drilling system is subjected to a variety of environmental loads that contributes to fatigue damage in a subsea WH and conductor system. The environmental loads acting on the system is shown in figure 4-1.

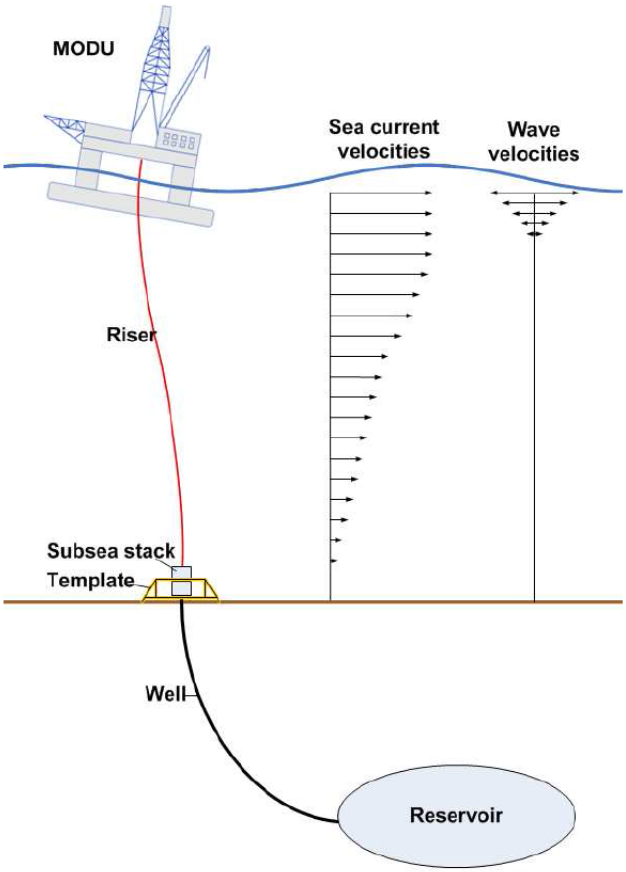

Figure 4-1 Environmental forces acting on the drilling system (DNV, 2011)

As mentioned earlier, heavier BOPs and longer periods where the riser is connected to the WH have increased the risk of high fatigue accumulation. Normally, offshore drilling operations are done using drilling risers and subsea BOP stacks deployed from offshore drilling units. A riser is used to get access to the well from the rig. The first step of the drilling operation, which is to install the WH and conductor system, is carried out in open sea. Once the WH is installed, the BOP stack and the drilling riser are connected and all further operations take place within the marine drilling riser. Throughout the life of a well, the WH system is a vital load-bearing structure, which supports the BOP, LMRP and the christmas tree at various times. The WH and conductor system is exposed to cyclic lateral loads from the drilling riser. As long as the riser

is connected to the WH, dynamic loads will be transmitted from the riser to the WH. These loads are generally driven by three factors (An et al., 2012):

- Severe wave conditions can cause vessel motions which are subsequently transferred to the top of the drilling riser.
- Waves can subject a direct hydrodynamic load in the riser resulting in riser motion.
- Under strong, steady currents the vortex shedding at the leeward side of the pipe may lock-on to the natural frequencies of vibration of the riser system, a phenomenon known as Vortex-Induced Vibration (VIV).

4.2 WAVES

Ocean surface waves cause periodic loads on all structures in the sea, regardless of whether they are fixed, floating, on the surface or deeper in the sea. Generally, ocean surface waves are distinguished in two states: sea or wind waves and swells. Sea or wind waves are waves that are being worked on by the wind that raised them and swells are waves that have escaped the influence of the generating wind. Normally, sea waves have a higher frequency than swell waves. Wind generated waves are changeable, varying both seasonally and regionally. Even though wind waves are very irregular and short crested, they can be seen as a superposition of many simple, regular harmonic wave components, were each component has its own amplitude, length and direction of propagation. This allows one to predict very complex irregular behavior in terms of the much simpler theory of regular waves (Journee & Pinkster, 2002).

By contrast to the stress fluctuations caused by current, wave-induced fatigue is a constant effect. Generally, wave-induced fatigue results in lower fatigue damage rates at the WH and conductor system. This is because wave loading will affect the upper part of the riser, creating loads and motions that are transmitted down to the WH. Inertia and hydrodynamic damping related to the lower riser portion will act to reduce these motions. Normally, the WH will experience a displacement range less than +-100 mm (Journee & Pinkster, 2002).

4.3 CURRENT

The term current describes the motion of the water. There are several factors responsible for the occurrence of current. One of these factors is the rise and fall of the tides. Tides create currents in the ocean near the shore and in bays and estuaries along the coast. These are called

tidal currents and are the only type of currents that change in a very regular pattern. Wind is another factor that drives ocean currents. Wind creates currents at or near the ocean's surface near coastal areas on a localized scale and in the open ocean on a global scale. A third factor, which drives currents, is thermohaline circulation. This is a process driven by the difference in water density due to temperature and salinity. Thermohaline circulation currents occur both in shallow and deep waters and move much slower than tidal and surface currents (National oceanic and atmospheric administration, 2010).

Current loads on the drilling system can cause VIV fatigue. In general, VIV becomes the conducting environmental load on drilling risers in water depths greater than 250 meters. VIV happens when the frequency of the vortices shed by current flow around the riser matches a natural frequency of the system. This will result in amplified lateral motions of the riser and may lead to accelerated fatigue and system degeneration. VIV can induce fatigue damage to the riser system and the WH and conductor system. VIV is often seen as a limiting factor during drilling operations because of the potential fatigue damage it can bring about. Because of this, operators may have to suspend drilling activity until the current speed reduces and lock-on terminates (An et al., 2012).

CHAPTER 5

5 FATIGUE

In order to understand why fatigue is a problem if it occurs in the WH and conductor system, it is necessary to understand how materials behave due to fatigue. According to ASTM (2011) the definition of fatigue is:

> *"The process of progressive localized permanent structural change occurring in a material subjected to conditions that produce fluctuating stresses and strains at some point or points and that may culminate in cracks or complete fracture after a sufficient number of fluctuations"*

This chapter contains a short introduction to what fatigue is and how it occurs. An overview of earlier accidents due to fatigue in the WH and conductor system is presented. A presentation of typical hotspots and their location is also given. In the last section, parameters effecting fatigue is described.

5.1 Introduction to Fatigue

Mechanical fatigue is dependent on the number of load cycles. It is difficult to define fatigue as only a material or structural problem. The inter material processes that take place in forming a nucleus crack are covered by material science. Global structural loading are causing these material processes which results in local stresses within the material. The structure's design and its capability to distribute load controls the stress level within the construction (Schijve, 2001).

Metal fatigue is the process of gradual degradation and eventual failure of a metallic specimen, component or structure. The phenomenon occurs under loads that vary with time and are lower than the static strength of the specimen, component or structure. These loads are cyclic in nature, but the cycles are not necessarily of the same size or clearly noticeable. The description of metal fatigue can be divided into two groups, metallurgical and mechanical. Metallurgical descriptions addresses the state of the material before, during and after application of fatigue loads. Mechanical descriptions are concerned with the mechanical response to a given set of loading conditions, e.g. the number of life cycles needed to cause failure. From an engineering point of view, where service behavior must be predicted, mechanical descriptions are more useful than metallurgical descriptions (Pook, 2007).

5.2 Fatigue Mechanisms

Fatigue is the weakening of a material caused by cyclic loading. An essential feature of fatigue is that the load is too small to cause instantaneous failure. Failure occurs after the material has experienced a certain number of load fluctuations. The most important load parameter is the stress or strain range, i.e. the difference between minimum and maximum stress in a load cycle. The fatigue process can be divided into three stages (Almar-Næss, 1985):

I Initiation or crack nucleation
II Crack growth
III Final fracture

According to DNV (2011), the fatigue life may be divided into two phases, crack initiation and crack propagation that eventually leads to fracture. For a non-welded component, crack initiation normally dominates the fatigue damage process, while for a welded component crack growth typically constitutes the largest portion of the fatigue life.

5.3 WELLHEAD AND CONDUCTOR FATIGUE

Fatigue is a phenomenon that only occurs when a material is subjected to cyclic loading. It can occur even when a structure experiences loads that generate stresses considerably below the elastic yield strength of the material. A subsea WH is exposed to constantly varying loads of high magnitude and therefore the fatigue response of the WH is of particular concern (Rimmer et al., 2013).

A subsea WH is typically subjected to dynamic loading from environmental forces. Normally, direct environmental loading on the WH is minimal and the majority of dynamic loading acting on the WH is generated from environmental forces acting on the drilling rig and the drilling riser (Evans et al., 2011). These forces are transmitted along the drilling riser and into the WH and conductor system and may lead to a buildup of high frequency elastic stress cycles in the system. If the system is exposed to these loads over an extended period, it may lead to eventual failure of a component in the WH and conductor system. Fatigue damage may accumulate at certain locations in the system frequently referred to as "fatigue hotspots". In the WH and conductor system these hotspots include welds and connectors located at the base of the WHH to a depth of 10-15 meters below the mudline (Greene & Williams, 2012). Typical fatigue hotspots along a WH and conductor system is illustrated in figure 5-1.

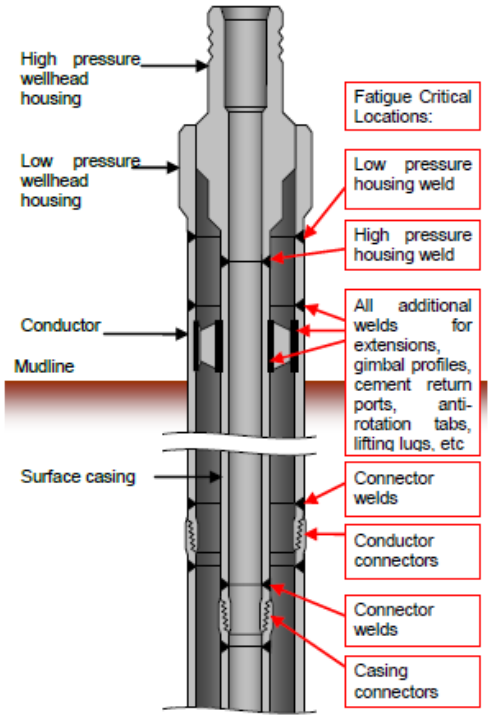

Figure 5-1 Typical WH and conductor system showing fatigue hotspots (Lim et al., 2013)

A fatigue failure of the WH system may have severe consequences. If the WH fails structurally its pressure vessel function will be lost and the well integrity will potentially be threatened. The structural load bearing function of the WH will also be affected (Reinås, 2012).

5.4 Parameters Effecting Fatigue Performance

5.4.1 Soil strength

Soft soils will increase the fatigue accumulation along the conductor and surface casing. Generally, in soft soils the peak bending moment will occur at 5 to 10 meters below the seabed surface. The conductor and surface casing connectors located at these depths becomes the most critical components with respect to fatigue. The magnitude of the bending moment will also be larger in softs soil because the lateral resistance of the soil becomes less, thus larger deflection of the BOP stack can occur. This results in further reduction in fatigue life. The peak bending moment in stiff soils will occur at a depth of 5 meters or less below the seabed surface. In stiff soils the greatest fatigue accumulation will occur at the welds and connectors near the seabed surface (Lim et al., 2012).

5.4.2 BOP stack size

Heavier and larger BOP stacks can worsen the fatigue lives along the wellhead, conductor and surface casing. The BOP stacks of the new 5th and 6th generation vessels are up to 1.6 times higher and 2 times heavier than the BOP stacks on older 3rd or 4th generation vessels. The increased size of the stack increases the fatigue loads in two ways (Lim et al., 2012):

- A larger height and weight will result in larger bending moments at the WH, conductor and casing for the same lateral displacement.
- A larger size increases the natural period of the BOP stack into the typical range of periods where waves and VIV motions occur. Larger BOP motions are generated if the period of the riser motions are close to the BOP stack natural period.

5.5 Previous Fatigue Failures of Wellheads

Dynamic loading of subsea WHs was first identified as a failure load in 1981. A structural fatigue failure of a surface casing/WH weld was experienced west of Shetland. At this time subsea development of offshore fields was in its early stages and since then the subsea technology has evolved into an established technology.

In 1989, Singeetham claimed that “The industry has experienced multiple field failures in the last 10 years, primarily at the bottom of the high pressure housing…” when discussing fatigue capacity on subsea WH systems. In 1983, Hopper reported a gross structural failure of the welded connection between the WHH and the surface casing due to fatigue. The failure was related to dynamic lateral loading from the drilling riser. In 1990, a paper addressing subsea field experience from the Beryl field in the UK part of the North Sea, King reported a fatigue failure of the first conductor casing connector (Reinås, 2012). In 2005, Statoil experienced significant lateral movements of the BOP on a subsea well during drilling operations in the North Sea. This WH had experienced lasting operations from drilling rigs, accumulating to approximately one year of operations. A parted conductor casing extension weld, caused by fatigue loading driven by drilling riser dynamic loads, explained the BOP movements (Reinås et al., 2011).

All these fatigue failures happened on subsea wells in service during drilling activities. They emphasize fatigue failure as a failure mechanism relevant to subsea wells. Failures have occurred in conductor casing connectors, in surface casing-WH welds, and in conductor-conductor housing welds. The two first failures happened in the early 1980s and a decade later King reported a new failure due to fatigue. 15 years later a fatigue failure happened again, this time in the North Sea. Since then, a distinguished Norwegian operator has suspected five cases of fatigue failures in subsea WH systems. Verification has not been obtained yet since the WHs have not been retrieved. The first of these failures was presented at the Underwater Technology Conference in Bergen in 2006. This incident proved that subsea WHs still can fail from fatigue loading by a connected drilling riser (Reinås, 2012).

CHAPTER 6

6 ORCAFLEX THEORY

The computer software used to perform the riser and conductor analysis in this thesis is OrcaFlex. In this chapter, the theory used in the calculations will be presented. OrcaFlex is a marine dynamics program developed by Orcina. The program is used to perform static and dynamic analysis of several offshore systems, including marine risers. OrcaFlex is a 3D non-linear time domain finite element program, which uses lumped mass elements to simplify the mathematical formulation and make the calculation efficient. This chapter is written according to the user manual in OrcaFlex (Orcina, 2013).

6.1 COORDINATE SYSTEMS

OrcaFlex uses one global coordinate system, GXYZ, where G is the global origin and GX, GY and GZ are the global axes directions. In addition to the global coordinate system, there are many local coordinate systems, generally one for each object in the model. In general, Lxyz is used to denote a local coordinate system and Exyz is the system for the line end orientation. The coordinate systems are all right-handed, with the Z-axis directed upwards. Figure 6-1 shows the global axes and a vessel with its own local vessel axes Vxyz. Positive rotations are clockwise when looking in the direction of the axis of rotation (Orcina, 2013).

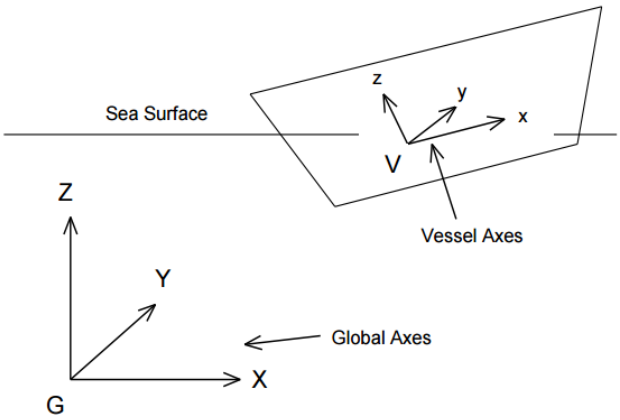

Figure 6-1 Coordinate system in OrcaFlex (Orcina, 2013)

The model of the riser and conductor is made up from lines, buoys and springs by use of the graphical user interface in the program. The process of the analysis can be divided into specific parts. The first step is to model the riser with the desirable dimensions. In the next step the environment must be chosen, i.e. waves and currents have to be established. The simulation can be run when the previous steps are specified and the wanted results can be obtained and evaluated. In the following chapters the element formulation, static and dynamic analysis used by OrcaFlex is presented.

6.2 LINE THEORY

OrcaFlex uses a finite element model for a line, as shown in figure 6-2. The line is divided into line segments that are then modelled by straight massless segments with a node at each end.

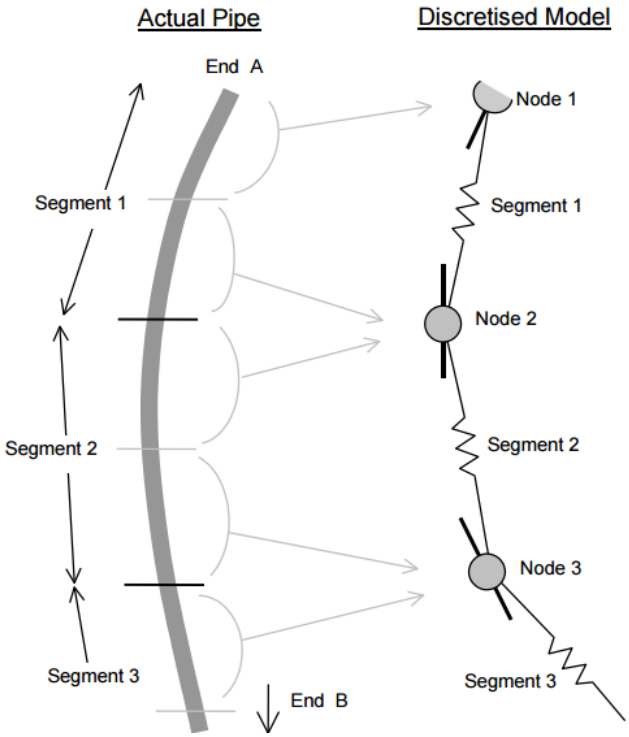

Figure 6-2 Line model in OrcaFlex (Orcina, 2013)

6.2.1 Nodes

The nodes model the weight, mass, buoyancy and drag properties of the actual line segments. Half of the segment length next to the node define the properties of the nodes. The node in each end is in itself modeled as a short rod that represents the combination of the properties of the half segment on each side of the node. Forces and moments are applied at the nodes (Orcina, 2013).

6.2.2 Segments

Each segment element models the axial and torsional properties of the line. The segment can be seen as being made up of two co-axial telescoping rods that are connected by axial and torsional spring/dampers. The axial spring/damper system is located at the center of each segment in the model, which applies an equal and opposite effective tension force to the nodes at each end of the segment. The bending properties are represented by rotational spring/dampers on either side of the node, spanning between the node's axial direction and the segment's axial direction. The system makes it possible to have different bending stiffness over the length of the model. The line's torsional stiffness and damping are modelled by the torsional spring/damper at the center of each segment, this applies equal and opposite torque moments to the nodes at each end of the segment. Inclusion of torsion to the system is optional, but if

torsion is not included in the analysis, the torsional spring/damper is missing and the two halves of the segments are free to twist relative to each other (Orcina, 2013).

6.3 STATIC AND DYNAMIC ANALYSIS

The calculation of forces and moments is performed in the following five stages: tension forces, bending moments, shear forces, torsion moments (if included) and finally total load. When the model is correctly constructed and the desired environment is applied the analysis can be run. The analysis consists of two parts, one static part and one dynamic part.

6.3.1 Static analysis

The static analysis has two main objectives: the first is to determine the equilibrium configuration of the system under weight, buoyancy, hydrodynamic, drag, etc. The second objective is to provide a starting configuration for dynamic simulation of the model. Static equilibrium is determined in a series of iterative stages. The initial positions of the vessel and buoys are defined by the data at the start of the calculation. These will in turn define the initial positions of the ends of any lines connected to them. The equilibrium configuration for each line is calculated with the assumption that the line ends are fixed. In the next stage the out of balance load acting on each free body is calculated and a new position for the body is estimated. This process is repeated until the out of balance load on each free body is zero (Orcina, 2013). OrcaFlex perform static analysis for each line in the model. The calculation is divided into two steps, where the first step calculates a configuration of the line and the second step calculates the true equilibrium position of the line. In the static analysis the first step is compulsory and the second step is optional (Orcina, 2013).

6.3.2 Dynamic analysis

The dynamic analysis is performed to simulate the motions of the model over a specified period. The motions can give forces, moments and displacements occurring in the system with the given load case. Before the main simulation, there is a built-up stage. During this built-up stage, the wave and vessel motions are smoothly ramped up from zero to full size. This is done to give a smooth transition from the static position to full dynamic motion. The build-up stage is numbered 0 and its length should in general be set to at least one wave period.

The calculation method in the dynamic analysis is done by solving the equation of motion. The equation of motion which OrcaFlex solves is as follows (Orcina, 2013):

$$M(p,a) + C(p,v) + K(p) = F(p,v,t) \qquad \textit{Equation 6-1}$$

Where M (p,a) is the system inertia load, C (p,v) is the system damping load, K (p) is the system stiffness load, F (p,v,t) is the external load, p,v and a are the position, velocity and acceleration vectors respectively and t is the simulation time.

In OrcaFlex, the dynamic analysis can be performed in two ways, explicit and implicit. Both systems recompute the system geometry at every time step, i.e. the simulation takes full account of all geometric non-linearities. The explicit method uses forward Euler with a constant time step. Static analysis give the initial positions and orientations of all objects in the model. The forces and moments acting on each free body and node are then calculated, the equation of motion is then formed for each free body and each line node (Orcina, 2013):

$$M(p)a = F(p,v,t) - C(p,v) - K(p) \qquad \textit{Equation 6-2}$$

Equation 7-2 is solved for the acceleration vector at the beginning of the time step, and then integrated using forward Euler integration. This integration gives the position and orientation of the nodes and the free bodies at the end of the time step. This process is repeated throughout the simulation time.

For the implicit method the calculation of forces, moments, damping, mass etc. are done in the same way as for the explicit method. The integration is done by use of the Generalized-α integration. Then the system equation of motion is solved at the end of the time step (Orcina, 2013).

6.4 LOADS

It is important to be aware of the loads that affect the system to be able to make the model as similar to the reality as possible. The system may be affected by different types of loads, including environmental, functional, accidental etc.

6.4.1 Waves

The model is subjected to waves in the dynamic analysis. OrcaFlex has several options for the implementation of waves in the model. Each wave train can be regular wave, random wave or specified by a time history file. OrcaFlex offers the following choices for regular wave modeling: long-crested linear Airy wave or non-linear waves using Dean, Stokes' 5th or Cnoidal wave theories. The waves are specified in terms of height, period and direction of propagation (Orcina, 2013).

In OrcaFlex, a random wave is a superposition of a number of regular linear waves with different heights and periods. The user has to specify the frequency spectra to model the random wave. The wave specter shows how the energy is distributed over the frequency occurring in the sea. For random waves OrcaFlex offers five standard frequency spectra: JONSWAP, ISSC, Ochi-Hubble, Torsethaugen and Gaussian Swell (Orcina, 2013). In the Norwegian Sea and the North Sea JONSWAP or Torsethaugen spectrum represents the design sea state.

The Torsethaugen spectrum is a double peaked spectrum best suited to North Sea conditions. Originally, the Torsethaugen model was established by fitting two JONSWAP shaped models to average measured spectra from the Norwegian Continental Shelf (Torsethaugen & Haver, 2004). This spectrum can represent sea states that include both a remotely generated swell and local wind generated waves. For this spectrum, the input values in OrcaFlex are wave period and wave height.

The JONSWAP spectrum was developed from the results of the Joint North Sea Wave Project and is created based on the Pierson-Moskowitz spectra. The spectrum applies to wind generated waves in the JONSWAP area (Thoft-Cristensen et al., 2012). Required input values for this spectrum in OrcaFlex are wave period, wave height and direction of propagation.

6.4.2 Hydrodynamic loads

To calculate the hydrodynamic loads on slender structures with a circular cross-section such as risers, Morison's equation can be applied. Morison's equation has been in use for more than 50 years, even though it has been considered controversial for many years. The equation is considered controversial principally because the drag force term is nonlinear. Morison's equation will give the forces on the riser with reasonable precision, if the diameter of the cylinder is small compared to the wavelength. Strip theory is applied to calculate the force per

unit length, in two dimensions. The hydrodynamic force acting normal to the pile is decomposed into two components, a drag force f_D and an inertia force f_I (Sparks, 2007):

$$f_H = f_D + f_I \qquad \textit{Equation 6-3}$$

The drag force is a result of the velocity of the flow past the riser and the inertia force is a result of the acceleration of the flow.

6.4.2.1 Drag force

Laboratory testing with steady flow has shown that the drag force for a cylinder varies with the square of the velocity. The expression for circular cylinders exposed to flow normal to its axis is given by (Sparks, 2007):

$$f_D = \frac{1}{2}\rho C_D D u|u| \qquad \textit{Equation 6-4}$$

Where ρ is the fluid density, C_D is the nondimensional drag coefficient, D is the diameter of the riser and u is the instantaneous velocity of the fluid (i.e. the velocity in the absence of the cylinder) normal to the cylinder axis. If the forces cause the riser to move laterally with a velocity v in the direction of the flow, the relative velocity must be used in equation 6-4. This is shown in the equation below (Sparks, 2007):

$$f_D = \frac{1}{2}\rho C_D D (u - v)|u - v| \qquad \textit{Equation 6-5}$$

6.4.2.2 Inertia force

Testing has also been done to investigate the inertia force due to fluid acceleration. For a stationary volume V of fluid density ρ subjected to acceleration flow the inertia force is given as (Sparks, 2007):

$$f_I = C_M \rho V \dot{u} \qquad \textit{Equation 6-6}$$

Where C_M is the inertia coefficient and $\dot{u}$ is the instantaneous acceleration of the fluid. The inertia force has two contributions, i.e. the hydrodynamic force acting on the displaced fluid in

the absence of the sphere (ρV$\dot{u}$) and an additional force due to the acceleration of the fluid relative the sphere (($C_M - 1$)ρV$\dot{u}$). If the sphere itself is moving with an acceleration $\dot{v}$ in the same direction as the fluid, the relative acceleration has to be used and results in the following equation (Sparks, 2007):

$$f_I = \rho V\dot{u} + (C_M - 1)\rho V(\dot{u} - \dot{v}) \qquad \textit{Equation 6-7}$$

Equation 6-6 and 6-7 apply to spheres in uniformly accelerated flow. If they are used to give the inertia force per unit length of a small-diameter cylinder, such as a riser, V is replaced by the external cross-sectional area A_e. The hydrodynamic force per unit length for a riser can be written as (Sparks, 2007):

$$f_H = \frac{1}{2}\rho C_D D(u - v)|u - v| + \rho A_e\dot{u} + (C_M - 1)\rho A_e(\dot{u} - \dot{v}) \qquad \textit{Equation 6-8}$$

6.4.2.3 Hydrodynamic force in OrcaFlex

OrcaFlex calculates the hydrodynamic forces on lines and buoys by using Morison's equation. The equation is the same as given in the previous sub-chapters but in OrcaFlex it is given for the whole length of the object instead of per meter. Morison's equation used in OrcaFlex is given by (Orcina, 2013):

$$F_w = (\Delta a_w + C_m\Delta a_r) + \frac{1}{2}\rho C_D A V_r|V_r| \qquad \textit{Equation 6-9}$$

Where F_w is the wave force, i.e. f_H. The first part of the equation, in the parentheses is the inertia force, where Δ is the mass of the fluid displaced by the body, a_w is the fluid acceleration and a_r is the fluid acceleration relative to the body. The last term in equation 6-9 is the drag force where V_r is the fluid velocity relative to the body and A is the drag area.

CHAPTER 7

7 METHODOLOGY AND MODELING

In this chapter, the methodology used for analysis of the drilling system will be given. The mechanical models and model built in OrcaFlex are also presented. To be sure that the model built in OrcaFlex corresponds with reality, a verification of the model is done and described in the last section of this chapter. The riser and WH and conductor system analysis is performed to simulate the reality as accurate as possible. To be able to perform calculations in a computer program, simplifications are needed, which in turn will cause limitations. This will make the model deviate from the reality. With this in mind, it is important to keep the physical properties correct in the transition from reality to model.

7.1 METHODOLOGY IN ISO 13624-2

ISO 13624-2 (2009) technical report is a supplement to the first part of the standard (ISO 13624-1) and gives methodologies and examples of how the riser analysis should be performed. In this chapter two methodologies for modeling of the drilling riser are presented: coupled and decoupled methodology. This section is in large extend written according to ISO-13624-2.

7.1.1 Coupled methodology

In the coupled analysis, see figure 7-1, the entire drilling riser system is modeled in the same analysis model. This includes the drilling riser, BOP stack, and the conductor/casing system. Current, waves and vessel offset can be applied directly to the entire drilling riser system using this method. This can be used to predict the behavior of the riser down to the displacements of the conductor in the soil.

Figure 7-1 Coupled methodology (ISO 13624-2, 2009)

Coupled analysis allows for full interaction between applied vessel motions, hydrodynamics and soil behavior. The coupled model is required for a more refined design of the conductor/casing system (ISO 13624-2, 2009).

7.1.2 Decoupled methodology

Decoupled analysis is a two-stage procedure that involves modeling the drilling riser and BOP/conductor/casing separately as shown in figure 7-2. The first part of the model represents the system from the upper flex joint to the lower flex joint and includes the drilling rig, tensioner system and slip joint. The second part of this model consists of the LMRP, BOP stack and conductor/casing system. Loads at the end of the first model are then applied to the top of the second model to evaluate the behavior of the conductor and riser at the mudline. Normally, a decoupled analysis provides more conservative results along the conductor/casing than coupled analysis. Compared with coupled analysis, decoupled analysis is more time-consuming and tedious to perform. The reason for this is that it is necessary for the loads at the lower flex joint to be post-processed following each drilling riser analysis and then applied to the BOP/conductor/casing through a further analysis. Note should be taken for shallow water and stiff clay applications, as the decoupled model can give slightly unconservative results (ISO 13624-2, 2009).

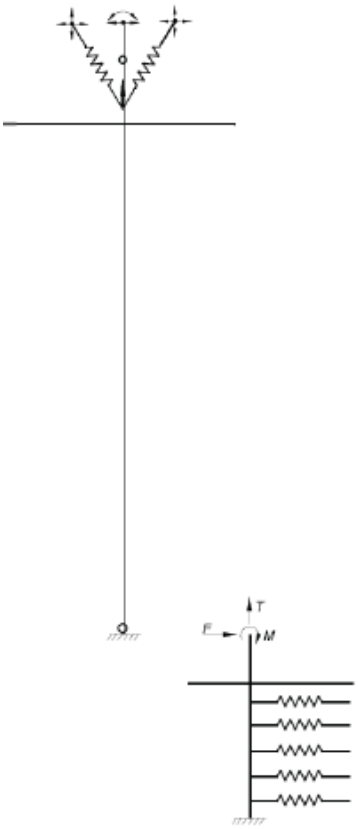

Figure 7-2 Decoupled methodology (ISO 13624-2, 2009)

In this thesis, the coupled methodology is most suited for the analysis. The analysis is performed in shallow water and the loads along the conductor are in focus.

7.2 MODEL DESCRIPTION

The simplest model of a tensioned riser is a straight pinned beam with tension acting as a force at the top. The WH and conductor system is structurally complexed with several interacting components. The system interacts with the surrounding soil, thus a structure-soil interface has to be included in the model (DNV, 2011). As mentioned in section 7.1, coupled methodology is chosen for the analysis in this thesis. The model, illustrated in figure 7-3, consists of a semisubmersible drilling rig, a tensioned riser, a BOP stack and the WH and conductor system. The 36" low-pressure housing provides an interface for the high-pressure housing. The BOP stack is located on top of the high-pressure housing.

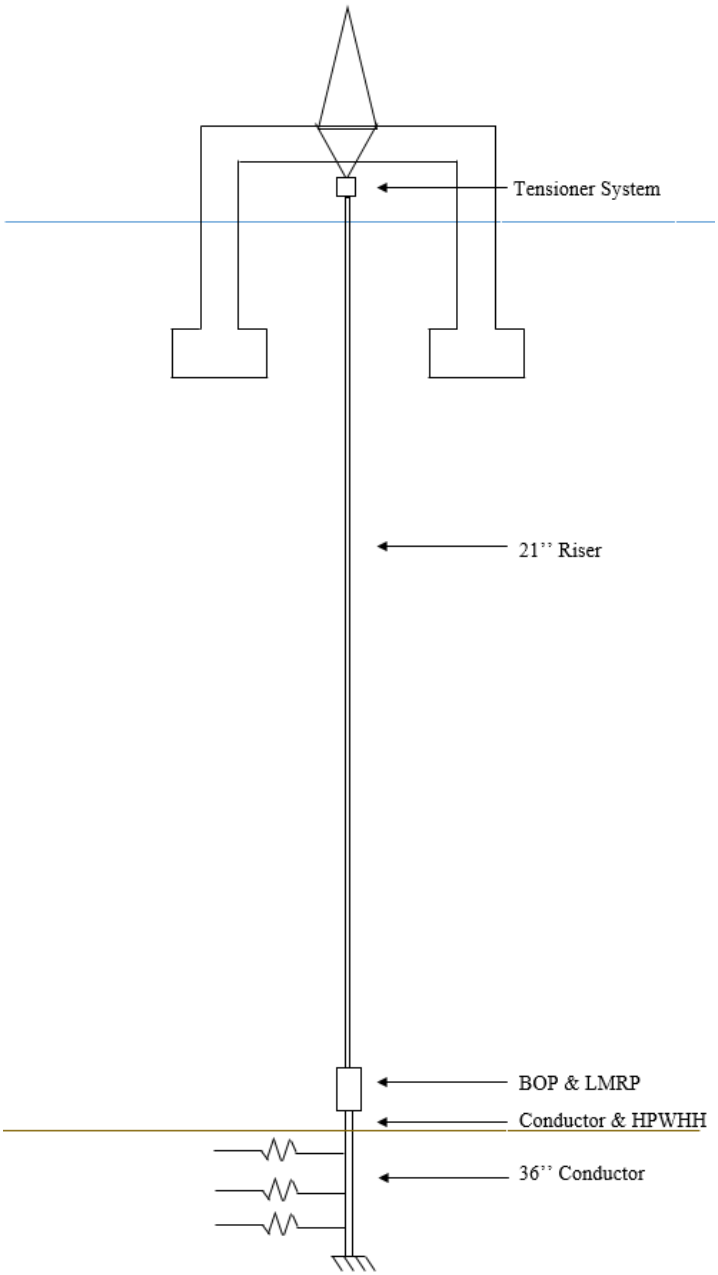

Figure 7-3 Model of the drilling system

Three different mechanical models are developed to perform the analysis: i) conventional installed conductor, ii) conductor installed inside the CAN, and iii) conductor installed inside the CAN with the WSF. The latter two are concepts developed by NeoDrill. The models are illustrated in figure 7-4.

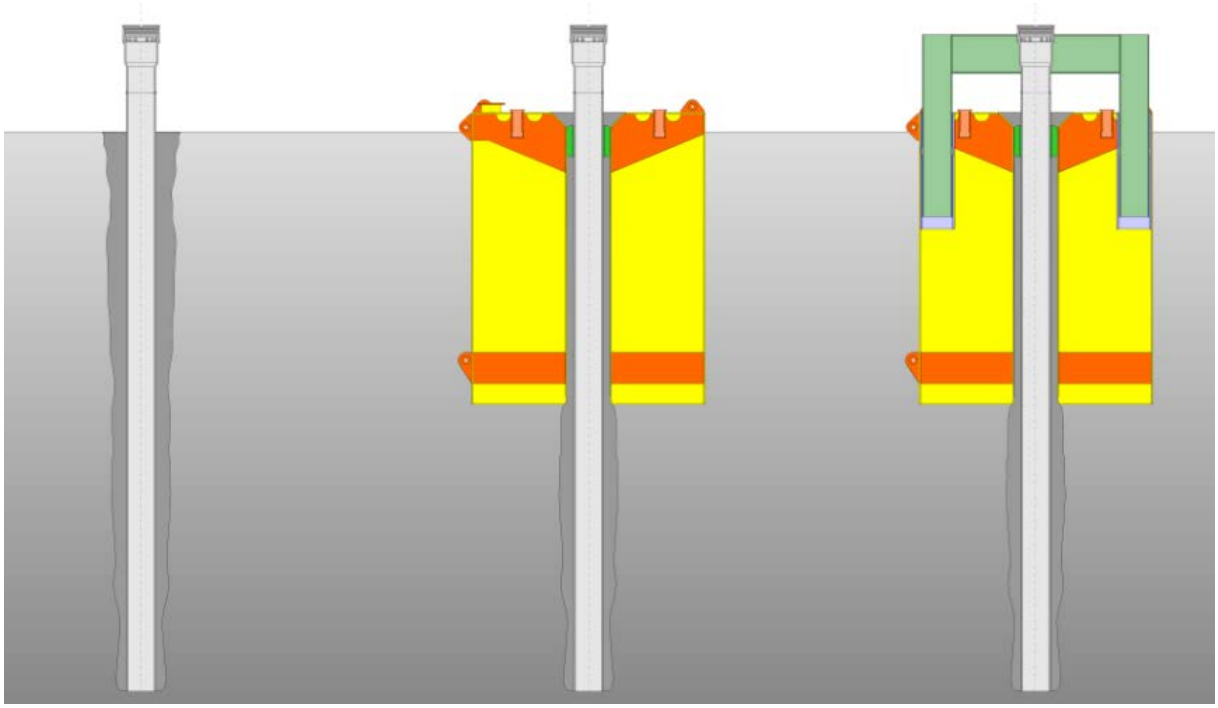

Figure 7-4 Illustration of a conventional installed conductor, the CAN and the WSF

The model to the left in figure 7-4 illustrates a conventional installed conductor, cemented to the seabed. The models in the middle and to the right are the two concepts developed by NeoDrill, i.e. CAN and WSF. The CAN supports the conductor from the seabed surface to a depth of 10 meters. It is designed to carry heavy BOPs and will provide the system with a very high lateral stiffness. The WSF, installed on top of the CAN, will support the high-pressure WH and gives the upper part of the system additional stiffness.

In this report the WH and conductor system is of interest, thus a mechanical model of the lower part of the system is created. Figure 7-5 illustrates the WHH, conductor housing and the soil stiffness modeled as springs. All three models have the same starting point, see figure 7-5, and modifications are done to account for the differences in the three scenarios. For all three models, it is assumed that the conductor is fixed at the lower end.

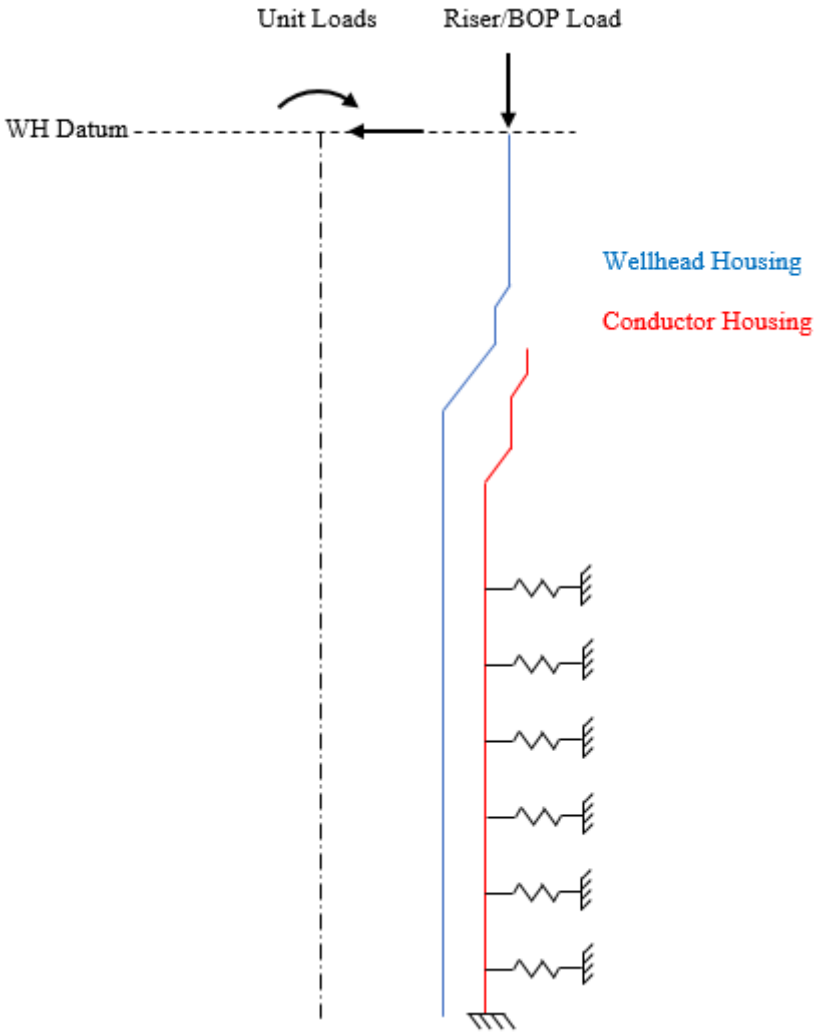

Figure 7-5 Mechanical model of WH and conductor system without the CAN and the WSF

Figure 7-5 shows the mechanical model of the first scenario, i.e. conventional installed conductor. In mechanical model 2, shown to the left in figure 7-6, the conductor is installed inside the CAN. Springs with high stiffness are used to model the properties of the CAN. It is assumed that the CAN has a stick-up height of 0.5 meters and that the CAN length is 10 meters, accordingly the first spring is located 0.5 meters above the seabed and the remaining springs are placed at intervals of 2 meters along the length of the conductor. All these springs have the same stiffness. The springs, which models the seabed, have the same stiffness as in the previous model. Mechanical model 3 is shown to the right in figure 7-6. The WSF gives the system additional stiffness. The stiffness of the WSF needs to be as high as possible to maximize load diversion. To obtain this very high stiffness an additional spring is placed near the top of the high-pressure housing, i.e. 1.5 meters above seabed surface. On recommendation from NeoDrill, this spring has a 10 times higher stiffness than the springs that represents the CAN.

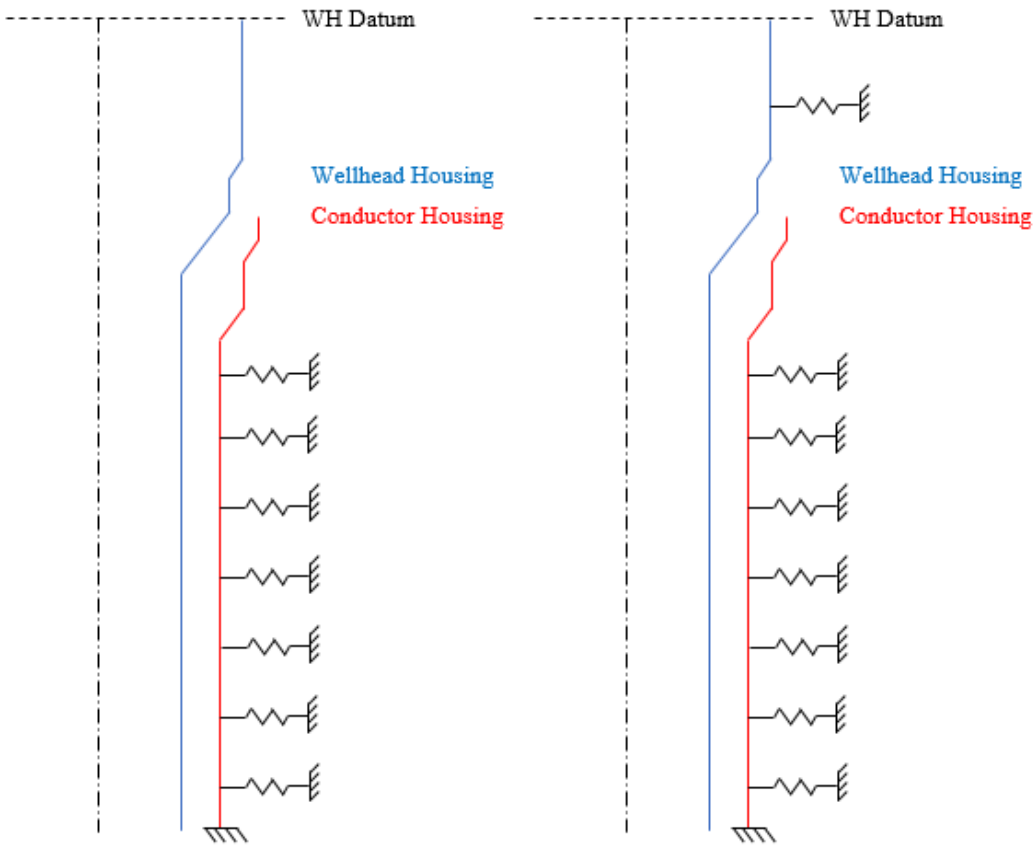

Figure 7-6 Mechanical model 2 (left) and mechanical model 3 (right)

In table 7-1 parameters used in the analysis are presented.

Table 7-1 Model details used in the analysis

Description		
Riser length	282	m
Riser OD	0.5334	m
Riser ID	0.4826	m
BOP+LMRP	250	Te
Conductor Length	42	m
Conductor OD	0.9144	m
Conductor ID	0.8382	m
Stick-up height	2	m
Soil Stiffness	50	kN/m
Spring Stiffness CAN	500E3	kN/m
Spring Stiffness CAN and WSF	5E6	kN/m

As mentioned in the beginning of this chapter, the WH and conductor system interacts with the surrounding soil, thus a structure-soil interface has to be included in the model. The soil supports the well, both vertically and horizontally. Resistance of the soil is dependent on the soil characteristics that are determined by in situ testing at different layers. Soil resistance is given by characteristic of the pressure (P) versus displacement (Y), this relationship is denoted P-Y curves. As figure 7-1 illustrates, the soil stiffness will be modeled as springs. The stiffness of the springs should be equivalent to the stiffness of the actual soil in the area of interest. In this thesis, P-Y curves are not available and a soil investigation to obtain values for different soil types is an extensive topic, thus not manageable in the time perspective of this project. A parametric analysis is done for the springs and presented in figure 7-7.

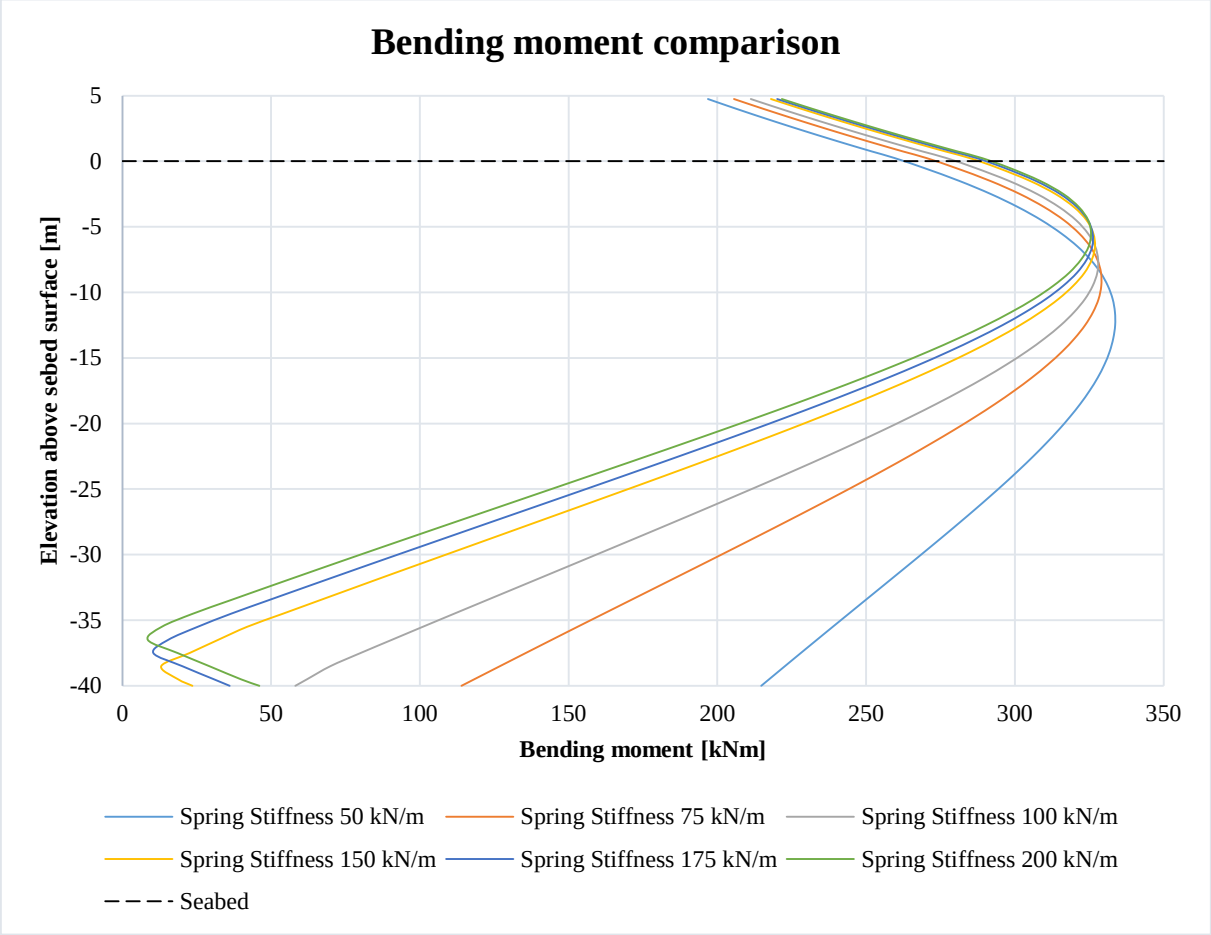

Figure 7-7 Bending moment comparison with different spring stiffness

Figure 7-7 shows how the bending moments change due to different soil stiffness. The BOP is not included in this plot, as this is a parametric analysis of the spring stiffness.

7.3 MODEL BUILT–UP IN ORCAFLEX

The model, illustrated in figure 7-8, built in OrcaFlex consists of a semisubmersible drilling rig, two buoys, two lines, and several links of spring/damper type. The water depth is assumed to be 300 meters.

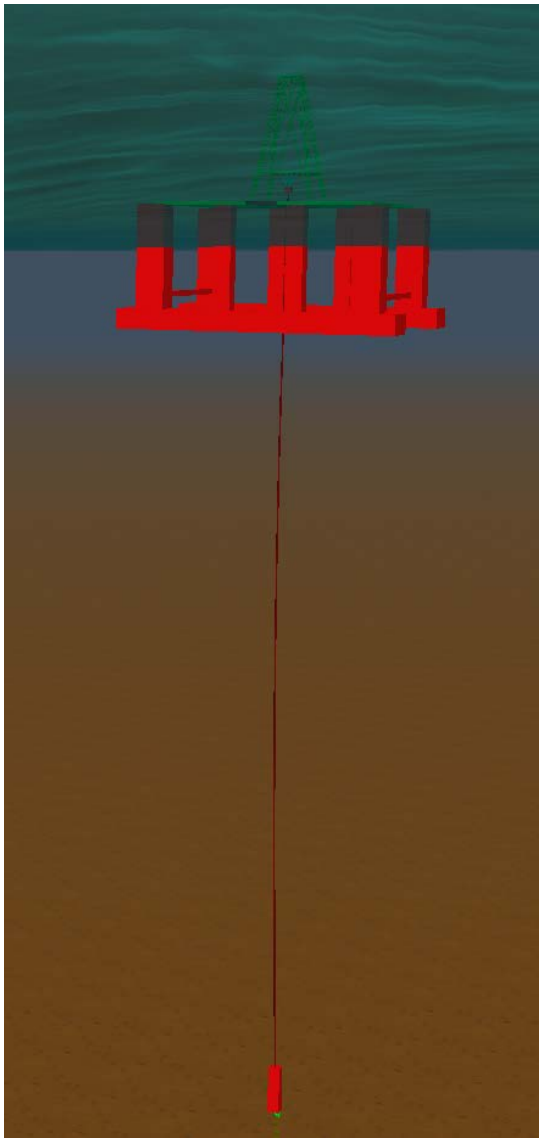

Figure 7-8 Model built in OrcaFlex

Three different models have been created to analyze the three different scenarios mentioned in section 7.2. The three models have the same starting point, some modifications are done to account for the differences in the three scenarios.

The drilling rig is obtained from example “B01 Drilling Riser” on the Orcina homepage (Orcina, 2015). The rig is a semisubmersible with eight columns, two pontoons and has a draft of 24.38 meters.

Four tensioners are modeled using links that functions as springs. The stiffness of the links is constant and there is no damping included. The tensioners are carrying the weight of the riser and are connected to the semisubmersible in the upper end and to the tension ring in the lower end. Required tension for each tensioner is calculated and presented in table 7-10.

The tension ring is modeled as a buoy with six degrees of freedom, meaning that moments and translation effects can be transferred to and from the buoy to the connected lines. The tension ring is given negligible properties, as its only purpose is to be a connection point for the tension lines and the riser.

The riser is modeled as a line and is connected to the tension ring in the upper end, 20 meters above mean sea level (MSL). It is assumed that the connection stiffness at the upper end of the riser is zero. The lower end of the riser is connected to the BOP stack. The flex joint reduces the bending moment in the lower end of the riser by allowing angular displacement between the riser and BOP stack. As the bending moment in the lower end of the riser is not of interest in this thesis, the flex joint has not been included in the model. Instead, the connection stiffness between the lower end of the riser and the BOP stack is assumed to be zero, thus zero bending moment will occur in this area. Torsion is not included in the riser line.

A 6D buoy is used to model the LMRP and BOP. The component is modeled as a body with six degrees of freedom. Hydrodynamic forces are calculated using Morison’s equation as for lines (Orcina, 2013). The BOP stack functions as a connection point for the riser and the conductor. The properties for the BOP stack are given in table 7-2.

The conductor is connected to the lower end of the BOP stack. It is modeled as a line and is assumed to have infinity connection stiffness at the upper end. Translations and moments are transferred from the BOP stack to the conductor. In the lower end of the conductor, connection stiffness is assumed infinite, i.e. the lower end is fixed to the soil. The properties for the conductor are given in table 7-2.

The seabed stiffness is set to zero, as the stiffness of sediments is preserved by using springs in the model. Several links of spring/damper type is used to model the seabed stiffness. Each link is attached to the conductor in one end and fixed to the soil in the other end. The first link is located at the seabed and the remaining links are placed at intervals of 2 meters along the entire length of the conductor. The same type of links are used to reproduce the physical properties of the CAN and the WSF. The locations of the links are the same as explained in section 7.2 and the stiffness is given in table 7-1.

7.3.1 Data for input and analysis

Choices for analysis parameters, variable input, significant wave height, wave period and current profile is provided below.

7.3.1.1 Component data

Data used in calculations for the components and as input in OrcaFlex for geometry and mass is given in Table 7-2. During simulation the fluid content in the riser system is mud, with a density of 1.5 kg/m^3. The mud has not been included when calculating the weights in table 7-2.

Table 7-2 Component data in OrcaFlex

Component	OD [m]	ID [m]	Length [m]	Weight in air [kg]
Riser	0.5334	0.4826	302	96000
BOP Stack	4	0.476	16	250000
Conductor	0.9144	0.8636	42	35000

The stiffness of the springs used to model the CAN and the WSF is presented in table 7-3. These values are used for all results presented in Chapter 8.

Table 7-3 Different spring stiffness

Description	Spring Stiffness	
Conductor no CAN	50	kN/m
CAN	500E3	kN/m
CAN and WSF	5E6	kN/m

7.3.1.2 Environmental data

In table 7-4, data used in calculations and input for environment in OrcaFlex are presented.

Table 7-4 Environmental data in OrcaFlex

Environmental data		
Sea Density	1025	kg/m^3
Kinematic Viscosity	1.35E-6	m^2/s
Sea Temperature	10	°C
Water Depth	300	m
Current	Variable with depth	-
Wave	Random	-
Spectrum	JONSWAP	-
Direction	180	deg

It is assumed that the current will decrease linearly with depth. The surface current is set to 1 m/s and the current reduces with 0.25 m/s for every one hundred meter, see table 7-5.

Table 7-5 Input data for current in OrcaFlex

Depth	Current Factor	
0	1	m/s
100	0.75	m/s
200	0.50	m/s
300	0.25	m/s

The significant wave height and wave period is assumed to be 3.5 meter and 8 seconds respectively, see table 7-6. JONSWAP wave spectrum is chosen for the analysis, as this spectrum represents the design sea state in the Norwegian Sea.

Table 7-6 Input data for wave height and wave period in OrcaFlex

Description		
Significant Wave Height, H_s	3.5	m
Wave Period, T_p	8	s

For integration, the implicit method is chosen. The explicit method requires very small time steps, which will lead to very long simulation time. The time step is set to 0.01 seconds.

The tolerance is the limit for the error accepted in the calculations. Orcina recommends the default tolerance value to be used.

Simulation time is reduced by the use of a build-up time at the beginning of the simulation. During this time, the wave dynamics, vessel motions and the current are build up smoothly from zero to full level. It gives a gentle start to the simulation, which reduces transient responses and avoids the need for long simulation runs. Generally, the build-up time should be set to at least one wave period. Negative time is shown during the simulation to indicate the build-up time (Orcina, 2013). As recommended by OrcaFlex, build-up time is set to one period, i.e. 8 seconds. Table 7-7 summarizes the abovementioned.

Table 7-7 Analysis specifications

Specification for analysis		
Integration Method	Implicit	-
Time Step	0.01	s
Maximum no. of iterations	100	-
Tolerance	25E-6	-
Build-up Time	8	s
Simulation Time	100	s

7.4 VERIFICATION OF ORCAFLEX MODEL

In this section, a verification of the model made in OrcaFlex will be given. Comparing analytical results to measurements of the real system is an effective method to verify the model and analysis. No measurements of the real system is done, consequently the results from the analysis will be compared with theory.

7.4.1 Total riser tension

According to DNV (2011), the applied top tension should be equal to the weight of the riser and mud, plus the over pull at the LMRP connector, less the buoyancy of the submerged riser. The riser weight and buoyancy are calculated from the lower end of the riser. Properties for the different elements included in the system is presented in table 7-8.

Table 7-8 Properties for different elements included in the system

Description		
Surfaced Riser	20	m
Submerged Riser	282	m
Riser OD	0.5334	m
Riser ID	0.4826	m
Steel Density, ρ_s	7850	kg/m^3
Mud Density, ρ_m	1500	kg/m^3
Water Density, ρ_w	1025	kg/m^3
Over pull	40000	kg

Table 7-9 contains the calculated weight of the entire riser, i.e. the surfaced part and the submerged part. Mud of density 1.5 kg/m^3 is included in the calculation.

Table 7-9 Accumulated weight of riser

Description		
Buoyancy	229	kg/m
Mud	274	kg/m
Mass Surfaced Riser	593	kg/m
Mass Submerged Riser	364	kg/m
Accumulated Mass	114508	kg

The required tension for the model is presented in table 7-10.

Table 7-10 Required tension at the upper end of the riser

Riser Tension upper end		
Riser	1123	kN
Overpull	392	kN
SUM	1515	kN

The required tension at the upper end of the riser is calculated based on weight of surfaced riser, weight of submerged riser and over pull at the lower end of the riser. Required tension at the upper end of the riser is 1515 kN, see last row in table 7-10.

Figure 7-9 illustrates the calculated effective tension compared to the results obtained in OrcaFlex. The calculated effective tension and the mean riser effective tension overlap almost perfectly.

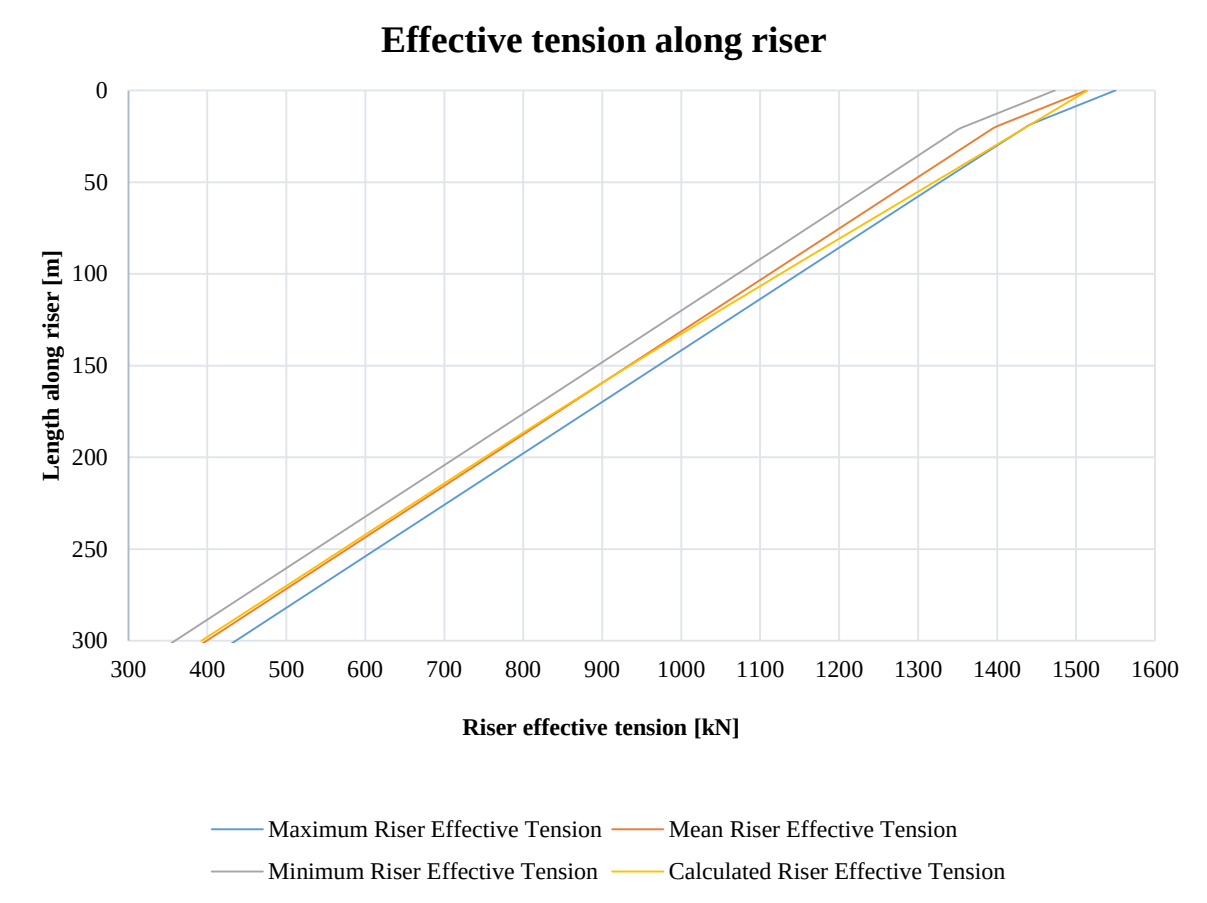

Figure 7-9 Effective tension along the entire length of the riser

The maximum and minimum riser effective tension, showed in figure 7-9, is due to waves and current acting on the riser. Waves and current will affect the system, thus the effective tension not beeing constant.

Figure 7-10 shows how the effective tension at the upper end of the riser fluctuates with time due to the environmental forces. During build-up time, the static effective tension matches the effective tension value given in OrcaFlex. The difference between the highest value and the lowest value is approximately 75 kN.

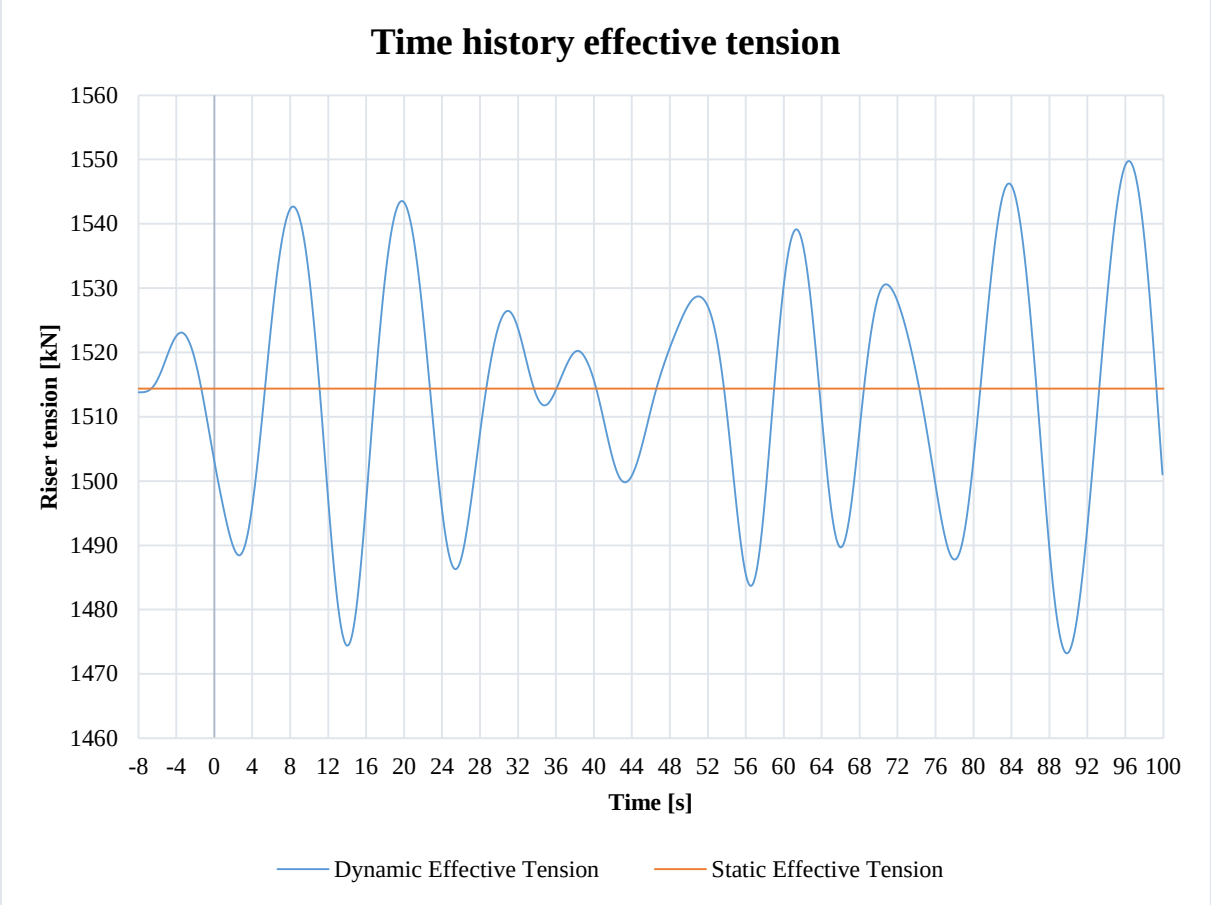

Figure 7-10 Time history of effective tension at upper end of the riser

7.4.2 Soil investigation

Soft soil gives greatly reduced lateral support to the WH and conductor system. The peak bending moment in soft soils will occur further away from the seabed surface compared to a soil with higher stiffness.

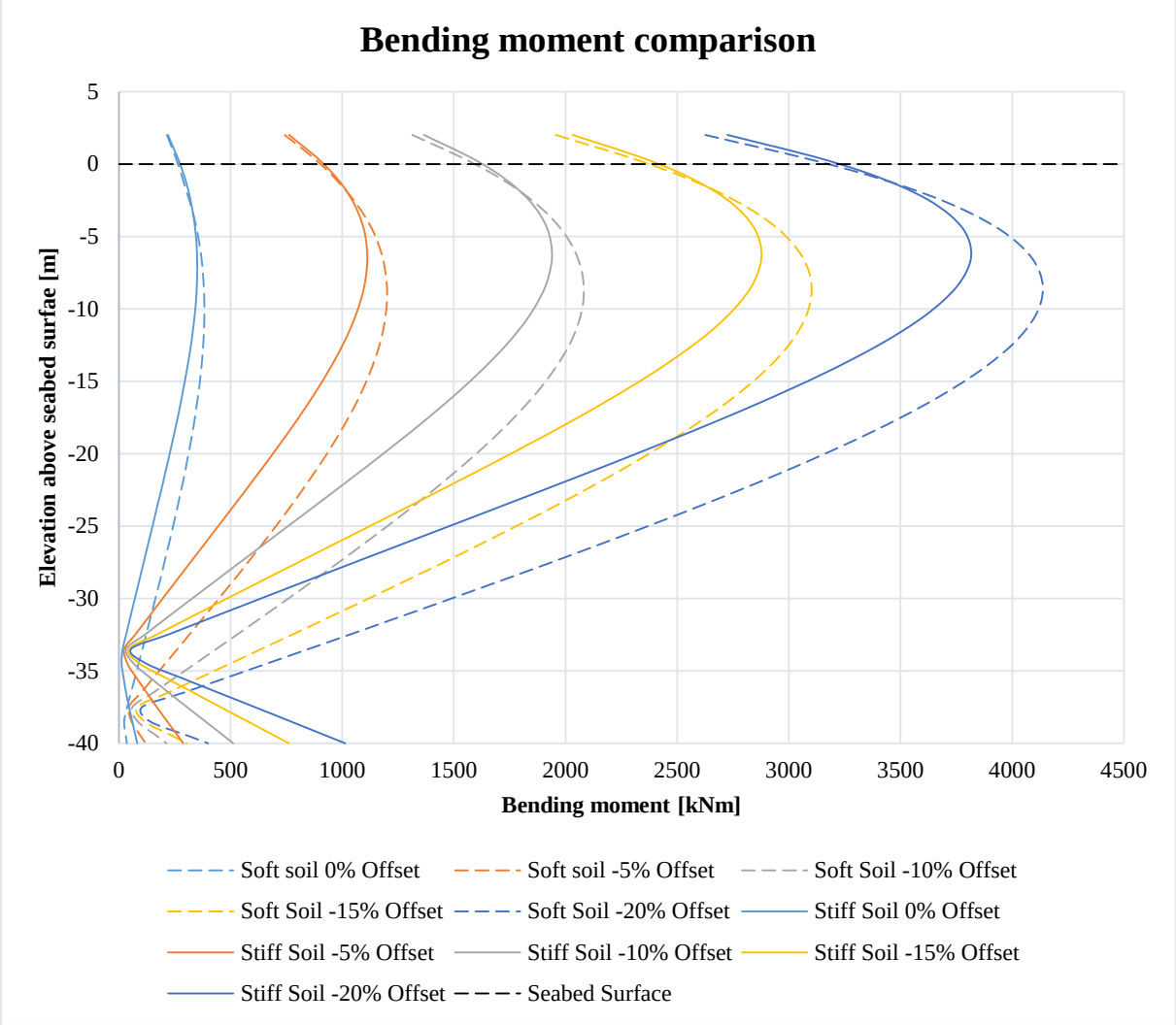

Figure 7-11 Bending moment comparison for different soil stiffness and lateral displacement of the rig

In Figure 7-11, it can be seen that the bending moments for different soil stiffness will change in magnitude and position. The dashed lines shows the bending moments in a soft soil, whereas unbroken lines shows the bending moments in a stiff soil. Offset of the rig is expressed as percent of water depth. The model built in OrcaFlex and the assumptions made for the stiffness of the springs corresponds to the theory presented in section 5.4

CHAPTER 8

8 RESULTS

In this chapter, results from the different analysis are presented. OrcaFlex can provide a huge number of different results. In this report the bending moments along the WH and conductor system is of interest, thus only these results will be presented. The first results presented in this chapter are bending moments along the WH and conductor system with different seabed stiffness and BOP stack weights. Thereafter, results for bending moments due to the CAN and the WSF are provided.

The position of the WH and conductor system places it in the region where high bending moments are generated. Theory in section 5.4 states that different soil stiffness will have an effect on the magnitude and location of the peak bending moment. A parametric analysis for different seabed stiffness is performed. Results are presented in Figure 8-1.

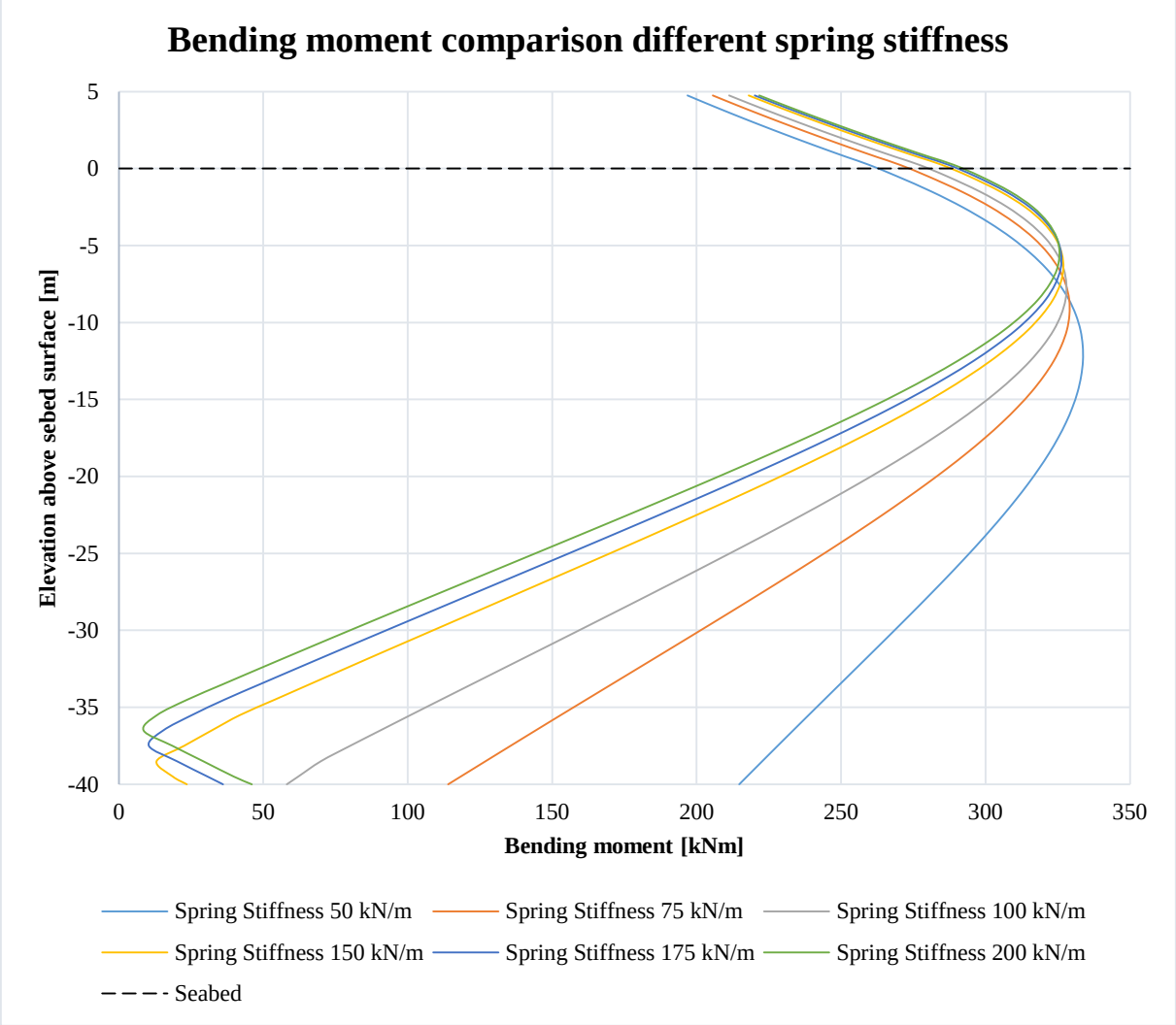

Figure 8-1 Bending moment distribution in different soil stiffness

The different lines in figure 8-1 represents the bending moments for different seabed stiffness. The largest bending moments will occur from the seabed surface to a depth of 10 to 15 meters below the seabed surface, see figure 8-1. When the stiffness of the soil is decreasing the maximum value of the bending moments are increasing. This effect will occur at a depth of 5 to 10 meters below the seabed surface, ref. figure 8-1. A higher soil stiffness changes the position of the largest bending moments. Additionally, the magnitude of the largest bending moments will decrease in soils with higher stiffness.

Normally, the bending moments decrease linearly with depth and becomes zero approximately 50 meters below seabed surface. In figure 8-1 this is not the case as the conductor is fixed at the lower end, causing a non-zero bending moment to occur in this area.

Between 35 and 40 meters below seabed surface, the bending moments corresponding to the three springs with the highest stiffness changes direction. The conductor will experience tension on one side and compression on the other side. This plot shows only positive values for the bending moments, thus compression and tension have the same sign.

When the lateral support decreases, larger deflections of the BOP may follow. The lateral displacement of the BOP depends on both the lateral support and the weight of the BOP stack. Figure 8-2 illustrates how different BOP weights affect the location and value of the largest bending moments.

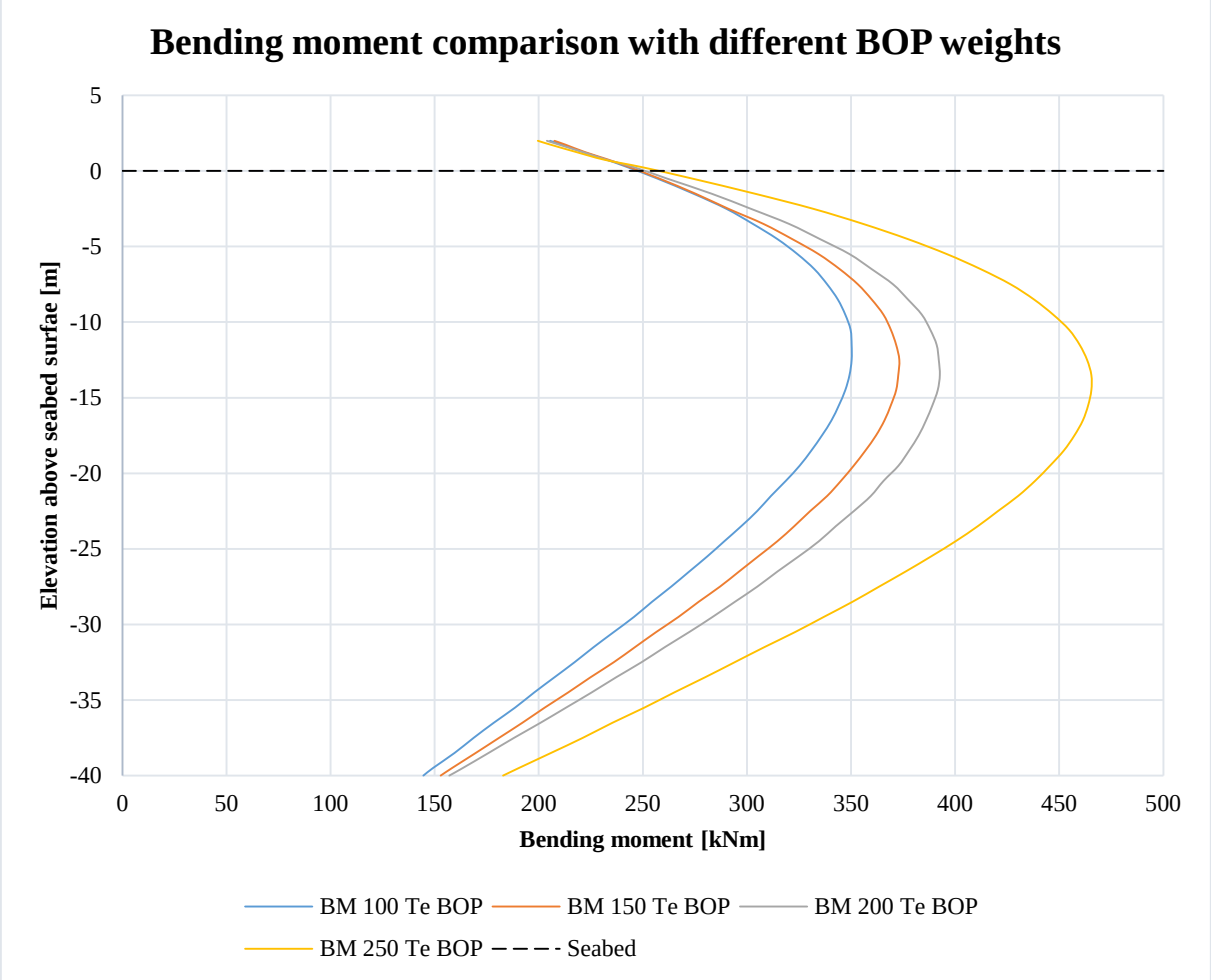

Figure 8-2 Bending moment comparison for different BOP weights in soft soil

Figure 8-2 indicates that there is a relationship between BOP weights and magnitude of the bending moment. A BOP stack weighing 250 tons will give a bending moment of approximately 470 kNm, while for a BOP weighing 100 tons the bending moment will be approximately 350 kNm, ref. figure 8-2.

An analysis of how the bending moments vary in different soils due to unequal BOP weights is presented in figure 8-3.

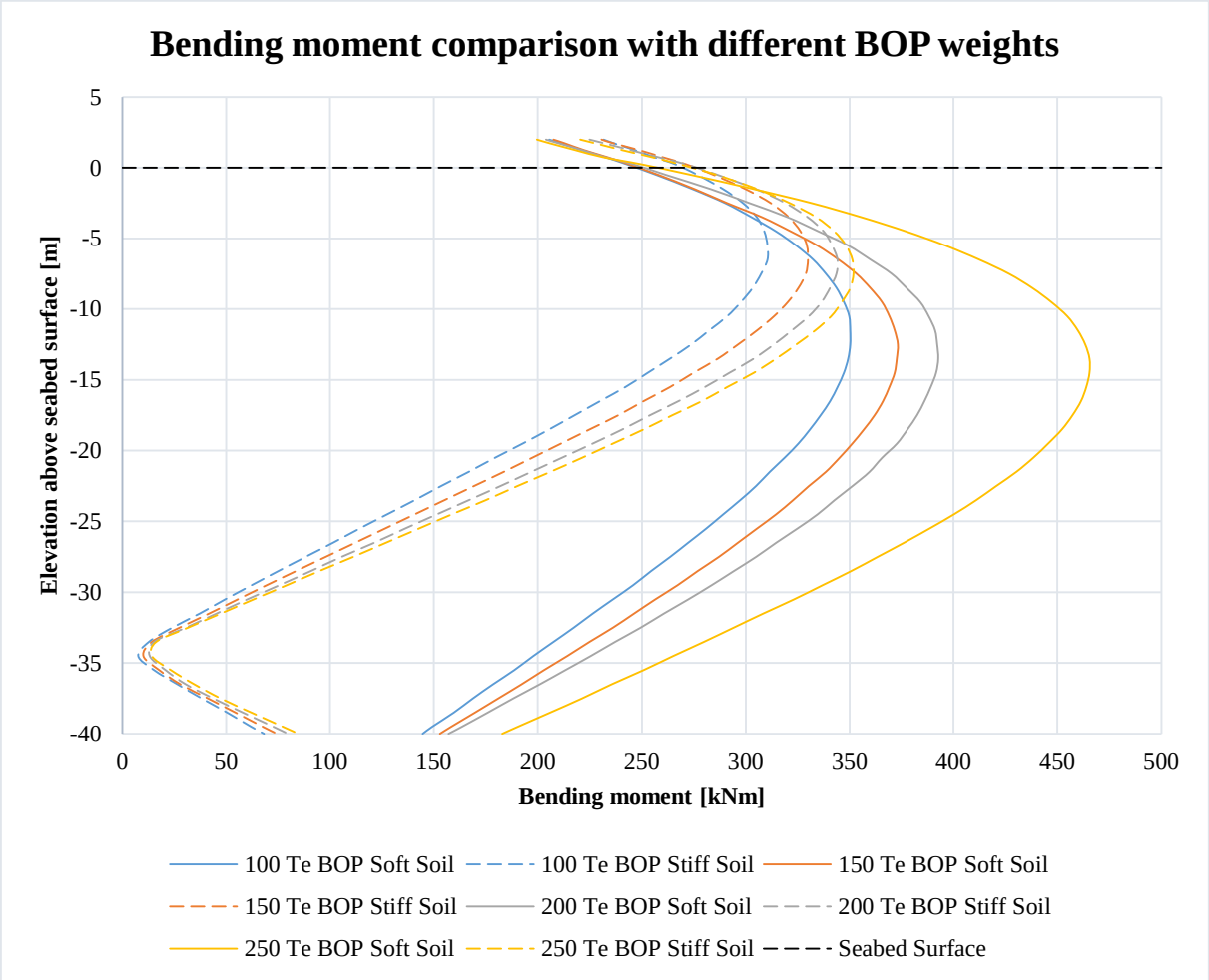

Figure 8-3 Bending moment comparison for different BOP weights in soft and stiff soil

A BOP weighing 200 tons will give a bending moment of approximately 390 kNm in soft soil. In stiff soil, the same BOP will provide a bending moment of 340 kNm. This gives a reduction of about 13%. In addition, the bending moments will occur closer to the seabed surface in stiff soils.

Figure 8-4 illustrates how the bending moments change due to the CAN. The CAN will give the system a very high lateral stiffness, thus reducing the bending moments located below the seabed surface. In the plot there is no lateral displacement of the rig, thus the bending moments occur due to waves and currents only.

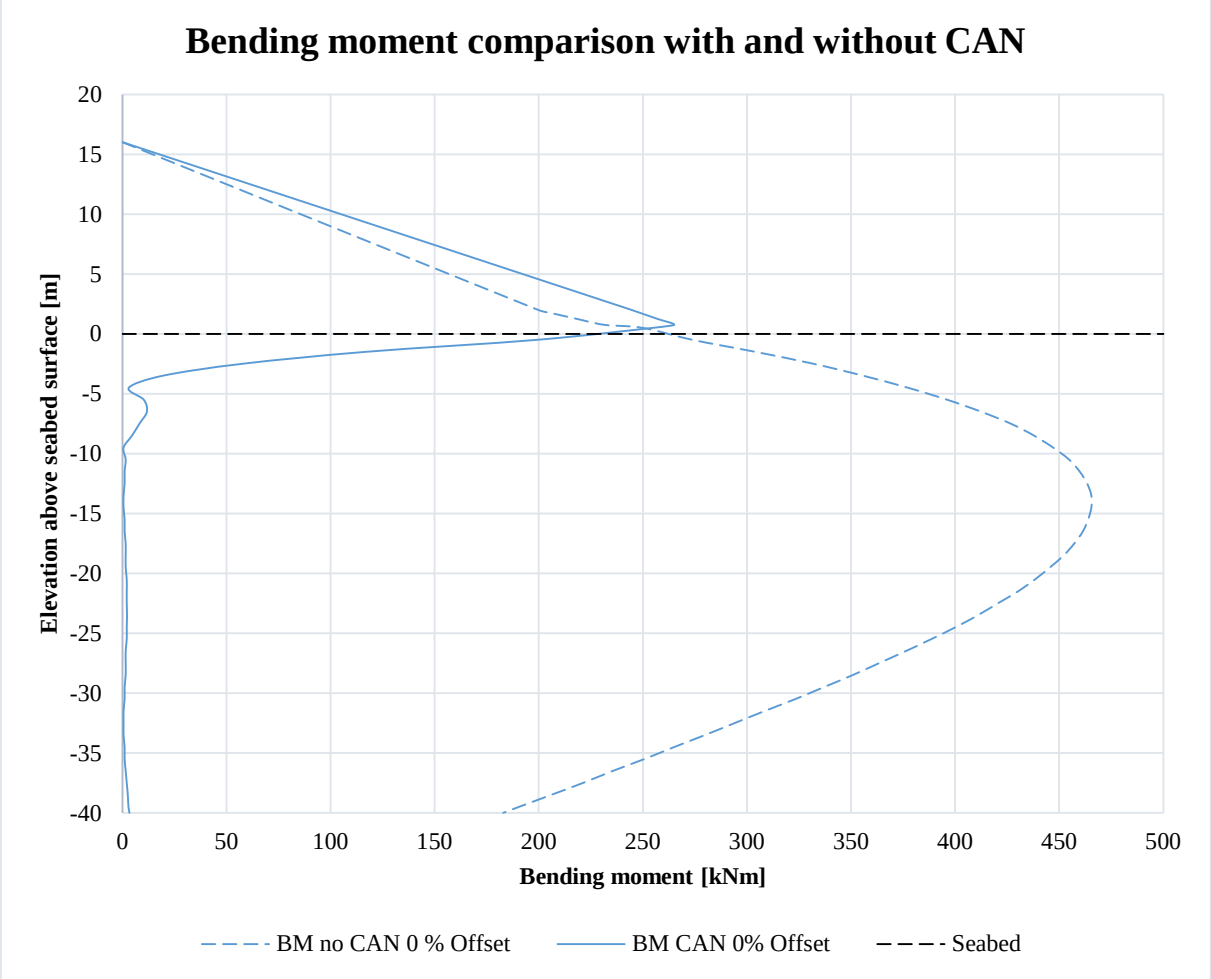

Figure 8-4 Bending moment comparison near seabed surface with and without the CAN installed

The figure shows a significant reduction of the bending moments located below the seabed surface. The maximum bending moment has a value of almost 470 kNm without the CAN installed. The bending moment is reduced to a value around zero because of the CAN. The bending moment will increase slightly on the top of the CAN. Central values from figure 8-4 are presented in table 8-1.

Table 8-1 Comparison of bending moments with and without the CAN installed at different points near seabed

Elevation above seabed surface [m]	Bending Moment no CAN [kNm]	Bending Moment with CAN [kNm]
0.5	231	265
-14.5	465	0.5

The percentage increase in bending moment on top of the CAN is approximately 15%. The peak bending moment at 14.5 meters below the mudline has a reduction of 99%.

In figure 8-5, it is illustrated how the bending moments change with the WSF installed. Compared to the case were only the CAN is installed, the WSF will give the system an even higher stiffness, ref. table 7-3. The bending moment below the WSF will have the same behavior as observed for the previous case, ref. figure 8-4. In the plot there is no lateral displacement of the rig, thus the bending moments occurs due to currents and waves alone.

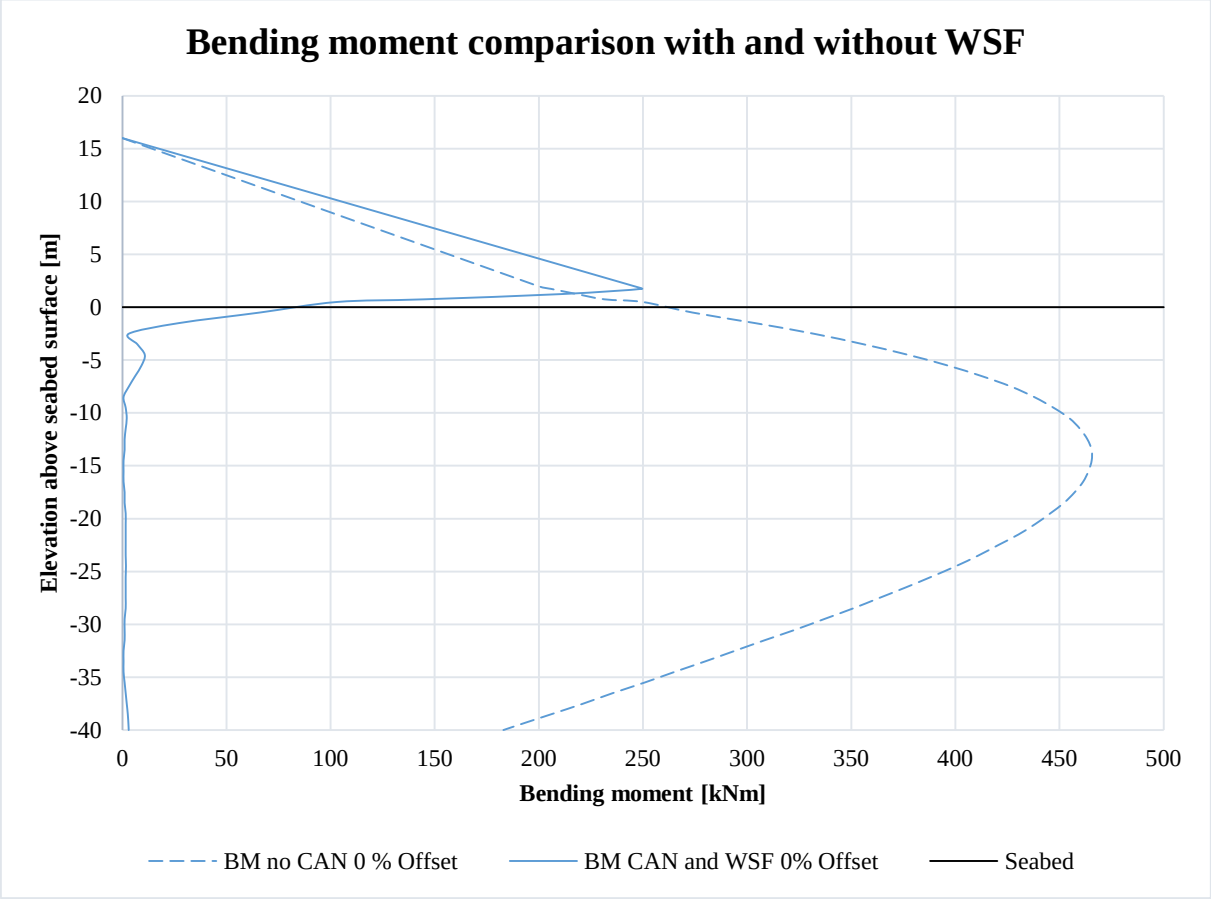

Figure 8-5 Bending moment comparison near seabed surface with and without the WSF installed

A significant reduction of the bending moment can be seen in figure 8-5. The bending moment will increase to some extent on top of the WSF. Key values from figure 8-5 are presented in table 8-2.

Table 8-2 Comparison of bending moment with and without the WSF installed at different points near seabed

Elevation above seabed surface [m]	Bending Moment no CAN [kNm]	Bending Moment with CAN and WSF [kNm]
1.5	205	250
-14.5	465	0.5

The increase in bending moment on top of the WSF is 22%. The peak bending moment at 14.5 meters below the mudline has a reduction of 99%.

The analysis for the CAN and the WSF has been run for three different lateral displacements of the rig: i) 0 meter offset, ii) -15 meters offset and iii) -60 meters offset. The lateral displacement is expressed as percent of water depth, i.e. 0%, -5% and -20%. Figure 8-6 shows how the bending moments, with and without the CAN installed, change due to different vessel offsets.

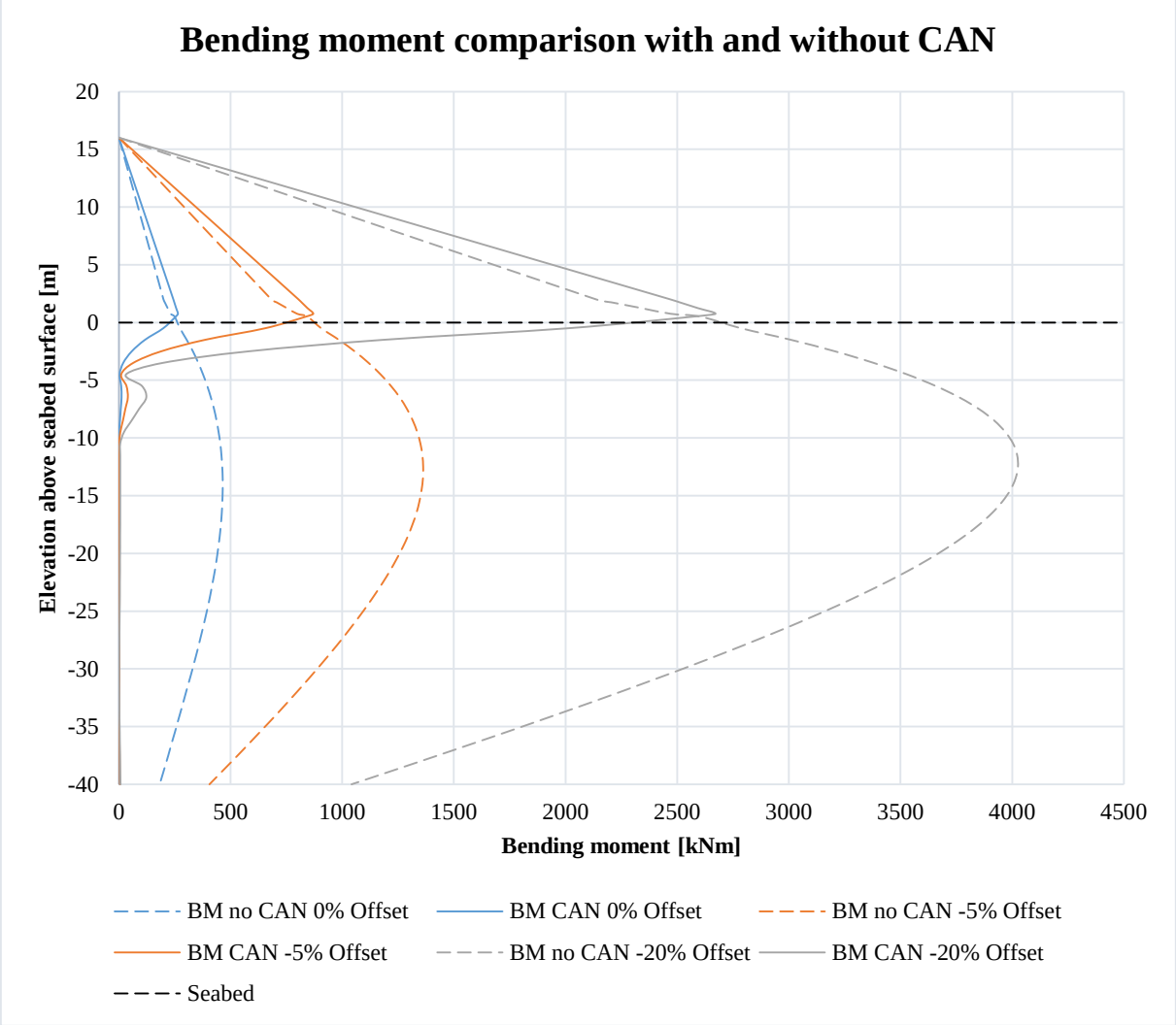

Figure 8-6 Bending moment comparison with and without the CAN installed for different vessel offsets

The magnitude of the maximum bending moments will increase because of larger offsets of the rig. The largest bending moments for 0% offset, -5% offset and -20% offset are approximately 490 kNm, 1300 kNm, and 4000 kNm, respectively. Although larger bending moments will occur due to rig displacements, the bending moments will still be reduced to a value around zero due to the CAN. A higher bending moment will occur on top of the CAN for all three displacements.

The plot in figure 8-7 shows how the bending moments, with and without the WSF, change due to different offsets. The observed changes are consistent with what has been illustrated previously in this chapter, i.e. the bending moments below seabed surface are reducing and the bending moments on top of the WSF are increasing slightly.

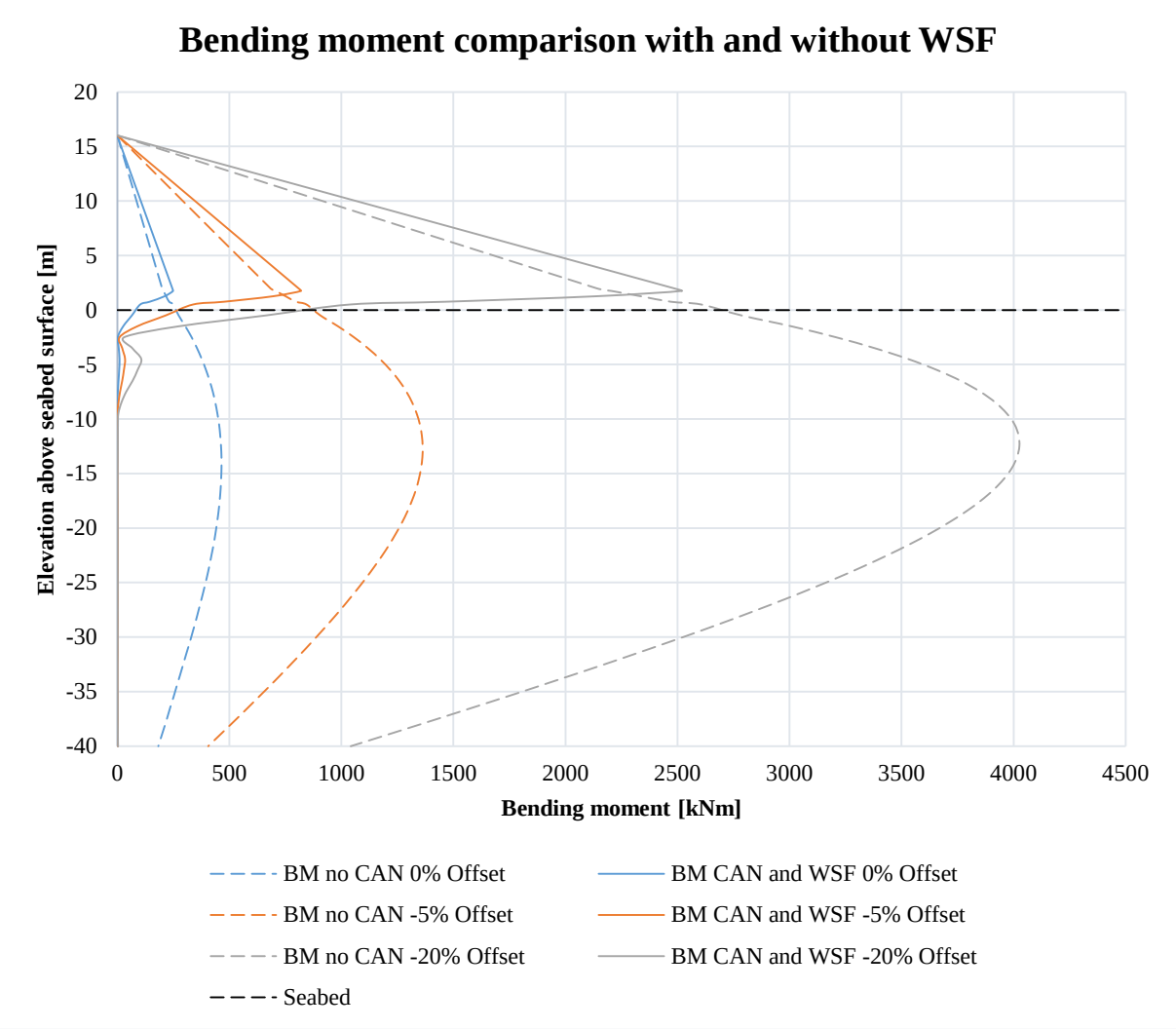

Figure 8-7 Bending moment comparison with and without the WSF installed for different vessel offsets

Central values from figure 8-6 and figure 8-7 are given in table 8-3 and table 8-4.

Table 8-3 Comparison of bending moments with and without the CAN installed for different lateral displacements of the rig

Elevation above seabed surface [m]	Offset as percent of water depth [%]	Bending moment no CAN [kNm]	Bending moment with CAN [kNm]
0.5	0	231	265
0.5	-5	798	870
0.5	-20	2470	2671
-14.5	0	465	0.5
-12.5	-5	1362	1.5
-12.5	-20	4025	5.6

Table 8-4 Comparison of bending moments with and without the WSF installed for different lateral displacements of the rig

Elevation above seabed surface [m]	Offset as percent of water depth [%]	Bending moment no CAN [kNm]	Bending moment with CAN and WSF [kNm]
1.5	0	205	250
1.5	-5	705	821
1.5	-20	2202	2521
-14.5	0	465	0.5
-12.5	-5	1362	1.5
-12.5	-20	4025	2

For a vessel offset of -20% the peak bending moment without CAN occurs around 12 meters below the seabed surface. Figure 8-8 shows a time history of the bending moment and how it fluctuates.

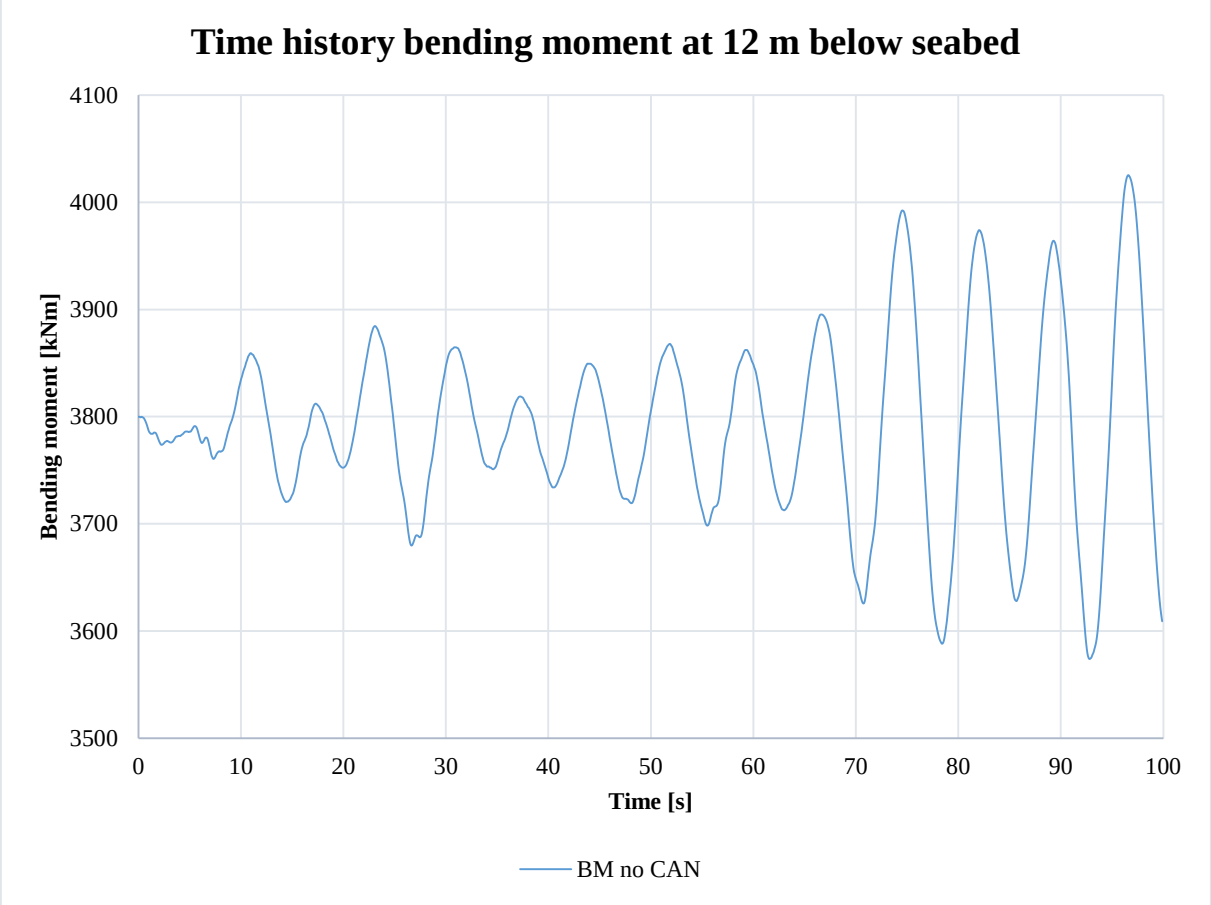

Figure 8-8 Time history bending moment with simulation time of 100 seconds

Figure 8-8 shows that the highest bending moment occurs after approximately 95 seconds. A new analysis was run for 200 seconds to check that there were no values exceeding the largest value reached in the simulation run for 100 seconds. The largest value reached is within the first 100 seconds of the simulation, see figure 8-9.

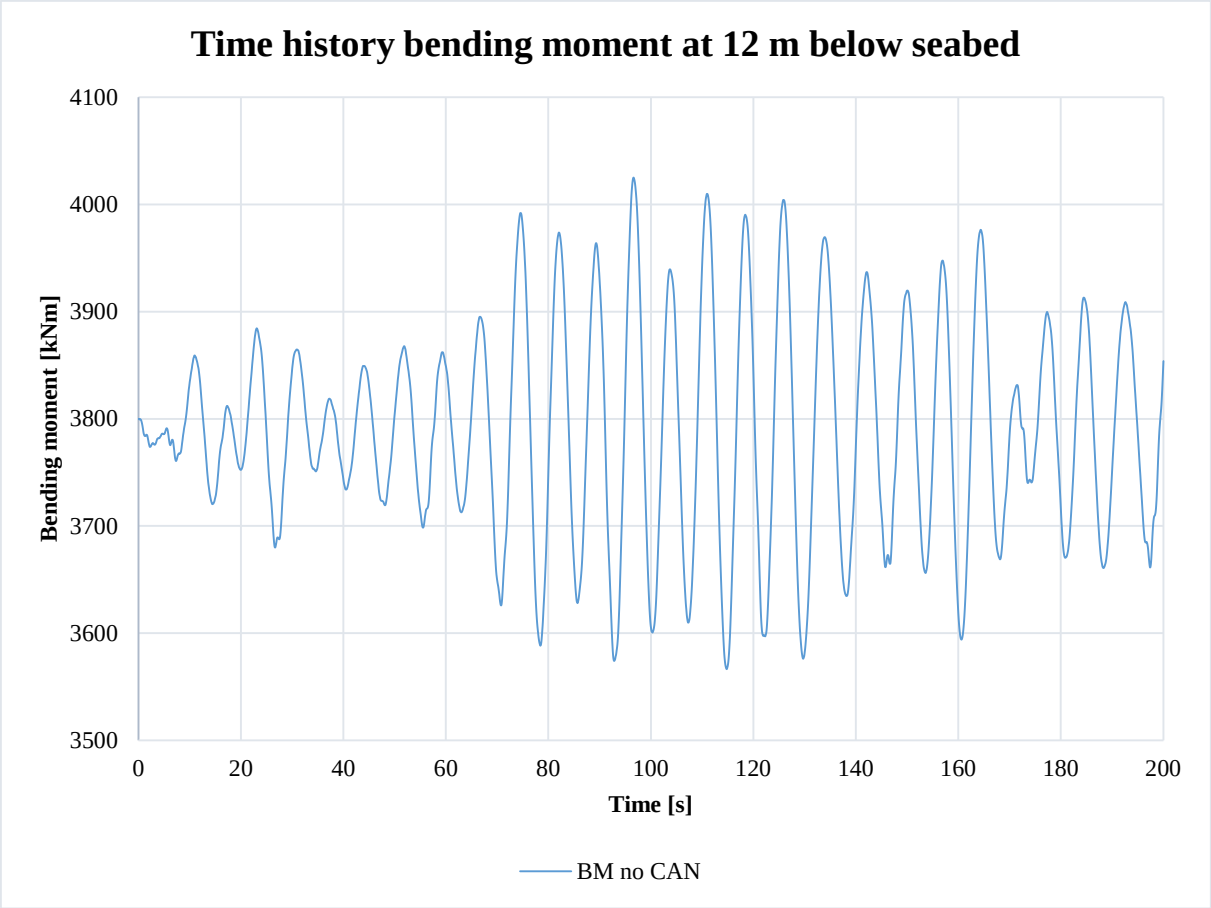

Figure 8-9 Time history bending moment with simulation time of 200 seconds

Figure 8-8 and figure 8-9 shows how the bending moments fluctuate in time due to waves and currents acting on the system.

CHAPTER 9

9 DISCUSSION

From the results in Chapter 8, there is a clear indication that the bending moments along the WH and conductor system will change due to different factors. As mentioned in section 5.4, the soil strength will affect the magnitude of the bending moment and the location of occurrence. Figure 8-1 shows that the largest bending moments in soft soils will occur approximately 5 to 13 meters below the seabed surface. Additionally, the figure shows that the magnitude of the largest bending moments is slightly larger in soft soils compared to stiff soils. The maximum bending moments in soft soils postpones the hotspots located in this area for fatigue loading. A higher soil stiffness makes the largest bending moments occur at a depth of 0 to 5 meters below the seabed surface, putting welds and connectors near the seabed surface at greatest risk of fatigue accumulation. Lim et al. (2012) states that in soft soils the largest bending moments will occur at a depth of 5 to 10 meters below seabed surface. In stiff soils, the largest bending moments occur at depths of 5 meters or less below seabed surface. The behavior of the bending moments observed in figure 8-1 shows consistency with the theory presented by Lim et al. (2012). The change in magnitude and location of the largest bending moments is most likely because the lateral resistance will change in different soils. When the lateral resistance of the soil decreases, larger deflections of the conductor pipe will occur, thus the magnitude of the bending moments will increase.

Normally, the bending moments will decrease with depth and will become zero around 50 meters below seabed surface. In figure 8-1 it can be seen that the bending moments have a non-

zero value at a depth of 40 meter below seabed surface. In this report, it is assumed that the conductor is fixed at this depth, i.e. the observed behavior in figure 8-1 is as expected.

Theory presented in section 5.4 states that in soft soils heavier BOPs will result in further reduction in fatigue life. In figure 8-3 a comparison of bending moments with different BOPs in soft and stiff soil is given. The bending moments increase significantly when the stiffness of the soil is decreasing. Ruf & Diestler (2013) states that in soft soils, the magnitude of the bending loads is larger as greater deflections of the BOP stack can occur. This is probably the observed effect seen in figure 8-3. As mentioned in the last paragraph, the lateral resistance will decrease in soft soils, thus leading to a larger lateral displacement of the conductor due to the heavy BOP. The risk of fatigue failure has increased significantly due to the use of 5th and 6th generations rigs with larger BOP stacks (Lim et al., 2013). This has probably increased the focus on fatigue failures of the WH and conductor system.

As stated by Sivertsen and Strand (2011) the CAN unit provides sufficient load capacity for safely carrying heavy BOPs, thus protecting the well from fatigue capacity "consumption" in the drilling phase. From the results in figures 8-4 and 8-6, it can be seen that the bending moments below the seabed surface decrease significantly due to the CAN. This large reduction below seabed surface is most likely because the CAN provides an increased bending stiffness. In figure 8-6, a comparison of the bending moments for different lateral offsets of the rig is shown. The reduction of the maximum bending moments in the case of 0% displacement, -5% displacement and -20% displacement is approximately 99% for all three displacements, see table 9-1.

Table 9-1 Comparison of bending moments with and without CAN installed

Elevation above seabed surface [m]	Offset as percent of water depth [%]	Bending Moment no CAN [kNm]	Bending Moment with CAN [kNm]
-14.5	0	465	0.5
-12.5	-5	1363	1.5
-12.5	-20	4025	5.6

The CAN will redistribute and change the position of the critical bending moments below the seabed surface. The large reduction and change of position will most likely reduce the fatigue

accumulation in the critical hotspots situated below the seabed surface. It is important to address that although the bending moments below the seabed surface are reduced, there will be a small increase of the bending moments located on top of the CAN. This behavior probably arises because the CAN will give the system a very high stiffness at this point. With this in mind, it is important to consider whether the most critical place for fatigue failure is below the seabed surface or at a short distance above the seabed. This cannot be done as a general consideration, but must be considered individually in each case. Table 9-2 shows how much the bending moments will increase on top of the CAN.

Table 9-2 Increase of bending moments on top of CAN

Elevation above seabed surface [m]	Offset as percent of water depth [%]	Bending moment no CAN [kNm]	Bending Moment with CAN [kNm]
0.5	0	231	265
0.5	-5	798	870
0.5	-20	2470	2671

On top of the CAN, the increase in bending moments for 0% offset, -5% offset and -20% offset is 15%, 9% and 8%, respectively. There is reason to believe that when the peak bending moments below the seabed surface decrease because of the CAN the stresses in the hotspots located in this area will also decrease. Reduction of stresses will lead to decreased fatigue accumulation. Accordingly, the critical hotspots located below the seabed will probably experience an increased fatigue life. On the other hand, a higher bending moment will occur on top of the CAN. A higher bending moment in this area exposes fatigue hotspots above the seabed surface for larger stresses, possibly leading to a reduction in fatigue life. The hotspots located beneath the seabed surface are two connector welds, conductor connectors and casing connectors, ref. figure 5-1 in chapter 5. Fatigue hotspots located above seabed surface, that are more susceptible to fatigue due to CAN, are the low-pressure housing weld, high-pressure housing weld and all additional welds for extensions, gimbal profiles, cement return ports, anti-rotation tabs, lifting lugs, etc.

From the results in figure 8-5 and figure 8-7, it can be seen that the bending moments will change additionally due to the WSF. Similar to the case were only the CAN is installed, a significant reduction of the bending moments is observed. The WSF changes the position of the

critical bending moments and it is likely to believe that the hotspots below the seabed surface will have an enhanced fatigue life.

The reduction of the maximum bending moments in the case of 0% displacement, -5% displacement and -20% displacement is about 99% for all three displacements, see table 9-3.

Table 9-3 Comparison of peak bending moments with and without the WSF installed

Elevation above seabed surface [m]	Offset as percent of water depth [%]	Bending moment no CAN [kNm]	Bending moment with CAN and WSF [kNm]
-14.5	0	465	0.5
-12.5	-5	1363	1.5
-12.5	-20	4025	2

The largest bending moments will occur on top of the WSF, which is 1.5 meters above seabed surface. The increase in bending moments due to the WSF is 21% for zero lateral displacement, 16% for -15 meters lateral displacement and 14% for -60 meters lateral displacement, see table 9-4.

Table 9-4 Increase of bending moment on top of the WSF

Elevation above seabed surface [m]	Offset as percent of water depth [%]	Bending moment no CAN [kNm]	Bending Moment with CAN and WSF [kNm]
1.5	0	205	249
1.5	-5	705	821
1.5	-20	2202	2521

The WSF changes the position of the critical bending moments and it is likely to believe that the hotspots below the seabed surface will have an enhanced fatigue life. Nevertheless, the higher bending moment that occurs on top of the WSF exposes critical components in this area for larger fatigue accumulation. Therefore, it is important to consider where an eventual fatigue damage is most problematic.

A comparison of the increased bending moment on top of CAN and on top of WSF shows that the WFS gives a greater percentage decrease in bending moments in the respective areas. There is a good reason to believe that this is due to the higher stiffness of the WSF. The stiffness of the WSF needs to be as high as possible to maximize load diversion.

Introduction of the WSF gives a reduction of the bending moments that occur between the CAN and the WSF, see table 9-5.

Table 9-5 Comparison of bending moments from top of the CAN to top of the WSF for zero lateral displacement

Elevation above seabed surface [m]	Bending moment with CAN [kNm]	Bending Moment with CAN and WSF [kNm]
1.5	248	249
1	256	144
0.5	254	102

The numbers presented in table 9-5 corresponds to zero lateral displacement of the rig. On the top of the WSF, i.e. 1.5 meters above seabed surface, there is a small increase of the bending moment. However, at 1 meter and 0.5 meters above the seabed surface the reduction is in the range of 45% and 60%, respectively. In appendix A, results for -5% and -20% lateral displacement are presented.

CHAPTER 10

10 CONCLUSION

One challenge when creating an analysis model is to reproduce the reality as accurate as possible. This can be difficult to do without all data available. In this report, a model was created with the aim to reproduce the physical properties of a real-life system. The objective was to investigate how the distribution and value of the maximum bending moments changed due to different factors and to identify a method to achieve an optimum distribution and position of critical bending moments.

In chapter 8, it is shown that the distribution of the bending loads will change due to variations in soil stiffness and BOP weights. The results show that in soft soils the largest bending moments will occur at a depth of 5 to 13 meters below the seabed surface. Additionally, the magnitude of the peak bending moment will increase in soft soils. In stiff soils, the largest bending moments will occur at a depth of 0 to 5 meters below the seabed surface. Moreover, the magnitude of the peak bending moments will decrease in stiff soils. These observations are consistent with studies done previously by other researchers, e.g. Lim et al. (2012), Ruf and Diestler (2013) and An et al. (2012). BOP weights will also have an impact on the bending moments. The results indicate that the maximum bending moments in soft soils will increase with heavy BOPs. This observation corresponds with the theory presented by Lim et al. (2012) which states that the combination of soft soils and heavy BOPs are two of the main reasons of large fatigue accumulation in critical hotspots located at a depth of 5 to 15 meters below seabed surface. The greatest risk of fatigue accumulation for stiff soils is at welds and connectors near the seabed surface (Lim et al., 2012).

From the results, there is a clear indication that the installation of the CAN and the WSF will change the distribution, position and values of the largest bending moments. Bending moments occurring at critical locations below the seabed surface are significantly reduced with the CAN and the WSF. Nevertheless, it is important to point out that larger bending moments will occur on top of the CAN or on top of the WSF. If the most critical hotspots are located below seabed surface, the CAN and the WSF will most likely provide a significant improvement in fatigue life of these hotspots. If this is not the case and the critical hotspots are located above the seabed, the CAN, and the WSF will probably expose these hotspots for somewhat increased fatigue damage. The CAN and the WSF gives the engineers a tool enabling an optimized system for maximum fatigue life below seabed surface. Without the CAN there is no possibility to change the characteristics of the seabed. However, it is difficult to identify one method to achieve an optimal distribution and position of bending moments, but it is possible to redistribute the bending moments and shift the problem to less critical locations in the system.

CHAPTER 11

11 SUGGESTIONS FOR FURTHER WORK

This thesis is not limited to any specific field. To get values that are more realistic, a model of a real-life system should be made, e.g. a more detailed drilling riser, include p-y curves in the model, obtain real-life data of waves and currents.

In order to calculate fatigue accumulation for the different hotspots located in the WH and conductor system a 3D FEM (finite element model) should be made. This model should be made according to DNV (2011) Wellhead and Fatigue Analysis Method. The modeling approach has been developed to perform fatigue analysis. The fatigue analysis should include a non-linear finite element analysis of the local response in the WH structure and a global load analysis which establish the loads acting on the well. The global analysis provides time series bending moments at WH datum and bending moment load histograms presenting the number of cycles for each load range. The fatigue damage is then calculated using rainflow counting in the case of stress time series or by summation of damage from each block in the case of stress histograms.

LIST OF REFERENCES

Almar-Næss, A. (1985). *Fatigue handbook : offshore steel structures*. Trondheim: Tapir.

An, P., Elletson, E., & Ward, P. (2012). Mitigation of wellhead and conductor fatigue using structural monitoring.

API. (1991). *Recommended Practices for Diverter Systems Equipment and Operations*: American Petroleum Institute.

API. (2010). Design, selection, operation and maintenance of marine drilling riser systems *API RP 16Q (R2010)*.

ASTM. (2011). Standard terminology relating to fatigue and fracture testing.

Bai, Y., & Bai, Q. (2005). Subsea pipelines and risersElsevier ocean engineering book series. Amsterdam: Elsevier.

Bai, Y., & Bai, Q. (2012). Subsea engineering handbook. Amsterdam: Elsevier/Gulf Professional Pub.

DNV. (2011). Wellhead fatigue analysis method (Vol. 2011-0063 / 12Q5071 - 26).

Evans, J., & McGrail, J. (2011). *An evaluation of the fatigue performance of subsea wellhead systems and recommendations for fatigue enhancements*.

Greene, J. F., & Williams, D. (2012). *The influence of drilling rig and riser system selection on wellhead fatigue loading.* Paper presented at the ASME 2012 31st International Conference on Ocean, Offshore and Arctic Engineering.

Hossain, N. (2011). *Fundamentals of sustainable drilling engineering*. New Jersey: Wiley-Blackwell.

ISO 13624-2. (2009). ISO/TR 13624-2 *Technical report. Deepwater drilling riser methologies, operations and integrity report*. Geneva: ISO.

Journee, J., & Pinkster, J. (2002). Introduction in ship hydro-mechanics. *Delft University of Technology*.

Lim, T. K., Koska, R., & Tellier, E. (2013). *Overcoming installation challenges to wellhead and conductor fatigue.* Paper presented at the ASME 2013 32nd International Conference on Ocean, Offshore and Arctic Engineering.

Lim, T. K., Tellier, E., & Howells, H. (2012). Wellhead, conductor and casing fatigue–causes and mitigation. *Proc. Deep Offshore Technology (DOT).*

Malm Orstad AS. (2015). Marine riser tension system. Retrieved 03.19, 2015, from http://www.malmorstad.com/products/marine-riser-tension-system

McCrae, H. (2003). *Marine riser systems and subsea blowout preventers* (1st ed.). Austin: Petroleum Extension Service.

National oceanic and atmospheric administration. (2010). Currents. Retrieved 31.05, 2015, from http://oceanservice.noaa.gov/education/tutorial_currents/welcome.html

NeoDrill. (2012). Subsea wellhead fatigue - learning and experience sharing preventing major accidents. Retrieved 04.05, 2015, from http://www.neodrill.no/uploads/kundefiler/WELLHEADFATIGUEPRES.pdf

NeoDrill. (2015). NeoDrill products & services Retrieved 17.03, 2015, from http://www.neodrill.no/index.php?sideID=33

Orcina. (2013). Orcaflex manual. Cumbria, UK

Orcina. (2015). OrcaFlex examples - B drilling risers. Retrieved 08.06, 2015, from http://www.orcina.com/SoftwareProducts/OrcaFlex/Examples/B%20Drilling%20Risers/index.php

Pook, L. P. (2007). *Metal fatigue : what it is, why it matters* (Vol. Vol. 145). Dordrecht: Springer.

Reinås, L. (2012). *Wellhead Fatigue Analysis : Surface casing cement boundary condition for subsea wellhead fatigue analytical models.* University of Stavanger, Norway.

Reinås, L., Hørte, T., Sæther, M., & Grytøyr, G. (2011). *Wellhead fatigue analysis method.* Paper presented at the ASME 2011 30th International Conference on Ocean, Offshore and Arctic Engineering.

Richbourg, M., & Winter, K. A. (1998). Subsea trees and wellheads: the basics.(Subsea Production Systems). *Offshore, 58*(12), 49.

Rimmer, A., Howells, H., & Ward, P. (2013). *Evaluation of wellhead fatigue using in-service structural monitoring data*.

Ruf, W., & Diestler, J. (2013). The growing use of structural monitoring as part of wellhead and conductor integrity management.

Schaer, M., & Gaschen, F. P. (2013). *Developments in marine transportation and exploitation of sea resources*. Chennai: Taylor & Francis.

Schijve, J. (2001). *Fatigue of structures and materials*. Dordrecht: Kluwer Academic.

Sheffield, R. (1982). *Floating drilling: equipment and its use*. Houston: Gulf Publishing Company.

Sivertsen, T. E., & Strand, H. (2011). *New well foundation concept, as used at a norwegian sea well*.

Sparks, C. P. (2007). Fundamentals of marine riser mechanics : basic principles and simplified analyses. Tulsa, Okla: Penn Well.

Stokvik, C. (2010). *An investigation of forces and moments from drilling risers on wellheads.* Norges teknisk-naturvitenskapelige universitet, Fakultet for ingeniørvitenskap og teknologi, Institutt for marin teknikk.

Subsea 1. (2010). Blow Out Preventer. Retrieved 03.19, 2015, from http://subsea1.com/index/search?content=bop&search.x=0&search.y=0

Thoft-Cristensen, P., & Baker, J. (2012). *Structural reliability theory and its applications.* Berlin: Springer Berlin Heidelberg.

Torbergsen, H.-E. B., Haga, H. B., Sangesland, S., Aadny, B. S., Sæby, J., Johnsen, S., . . . Lundeteigen, M. A. (2012). An introduction to well integrity. Retrieved 07.06, 2015 from:https://www.norskoljeoggass.no/Global/2013%20Dokumenter/Andre%20vedlegg/INTRODUCTION%20TO%20WELL%20INTEGRITY%20-%2004%20December%202012.pdf

Torsethaugen, K., & Haver, S. (2004). *Simplified double peak spectral model for ocean waves.* Paper presented at the Proceedings of the 14th International Offshore and Polar Engineering Conference, Toulon, France, May.

APPENDIX A

A. Bending moment comparison

Introduction of the WSF gives a reduction on the bending moments that occur between the CAN and the WSF. In this appendix bending moment values for -5 meters offset and -20 meters offset is given, see table 0-1 and 0-2.

Comparison of bending moments from top of the WSF to top of the CAN for -5 meters offset

Elevation above seabed surface [m]	Bending moment with CAN [kNm]	Bending Moment with CAN and WSF [kNm]
1.5	817	821
1	844	694
0.5	870	475

On top of the WSF, i.e. 1.5 meters above seabed surface there is an increase around 1%. However, at 1 meter there is a reduction around 17% and at 0.5 meter the reduction is around 45%.

Comparison of bending moments from top of the WSF to top of the CAN for -20 meters offset

Elevation above seabed surface [m]	Bending moment with CAN [kNm]	Bending Moment with CAN and WSF [kNm]
1.5	2509	2521
1	2591	2131
0.5	2671	1460

On top of the WSF, i.e. 1.5 meters above seabed surface there is an increase around 1%. However, at 1 meter there is a reduction around 18% and at 0.5 meter the reduction is around 45%.